Basement membrane diversification relies on two competitive secretory routes defined by Rab10 and Rab8 and modulated by dystrophin and the exocyst complex

Cynthia Dennis[1], Pierre Pouchin[1], Graziella Richard[1], Vincent Mirouse[1,*]

1) Institute of Genetics, Reproduction and Development (iGReD), Université Clermont Auvergne - UMR CNRS 6293 - INSERM U1103, Faculté de Médecine, 28 Place Henri-Dunant, 63000 Clermont-Ferrand, France
*contact: vincent.mirouse@uca.fr

The basement membrane (BM) is an essential structural element of tissues, and its diversification participates in organ morphogenesis. However, the traffic routes associated with BM formation and the mechanistic modulations explaining its diversification are still poorly understood. *Drosophila melanogaster* follicular epithelium relies on a BM composed of oriented BM fibrils and a more homogenous matrix. Here, we determined the specific molecular identity and cell exit sites of BM protein secretory routes. First, we found that Rab10 and Rab8 define two parallel routes for BM protein secretion. When both routes were abolished, BM production was fully blocked; however, genetic interactions revealed that these two routes competed. Rab10 promoted lateral and planar-polarized secretion, whereas Rab8 promoted basal secretion, leading to the formation of BM fibrils and homogenous BM, respectively. We also found that the dystrophin-associated protein complex (DAPC) associated with Rab10 and both were present in a planar-polarized tubular compartment containing BM proteins. DAPC was essential for fibril formation and sufficient to reorient secretion towards the Rab10 route. Moreover, we identified a dual function for the exocyst complex in this context. First, the Exo70 subunit directly interacted with dystrophin to limit its planar polarization. Second, the exocyst complex was also required for the Rab8 route. Altogether, these results highlight important mechanistic aspects of BM protein secretion and illustrate how BM diversity can emerge from the spatial control of distinct traffic routes.

Introduction

Basement membrane (BM) is a specialized extracellular matrix forming a complex sheet-like architectural meshwork that lines most of animal tissues, such as epithelium and muscle (Jayadev & Sherwood, 2017; Mouw et al, 2014). BM is critical for tissue development, homeostasis and regeneration, as exemplified in humans by its implication in many congenital and chronic disorders. Therefore, understanding its properties is a major issue for regenerative medicine (Bonnans et al, 2014; Chaudhuri et al, 2020). BM is assembled from core components conserved throughout evolution: type IV collagen (Col IV), the heparan-sulfate proteoglycan perlecan, and the glycoproteins laminin and nidogen. During development, the dynamic interplay between cells and BM participates in sculpting organs and maintaining their shape. Specifically, BM influences essential cellular processes (e.g. cell identity, growth, shape, and migration) through various cell surface receptors, such as integrins (Chaudhuri et al, 2020; Humphrey et al, 2014; Kyprianou et al, 2020; Munjal et al, 2021; Sherwood, 2021; DAC & Yamada, 2020). Reciprocally, cells constantly produce and remodel their BM, thus modifying their mechanical and biochemical microenvironment (Bonnans et al, 2014; Munjal et al, 2021; Palmquist et al, 2022). BM protein secretion shows some specificities, mainly because of the large size of the protein complexes (e.g. procollagen) that must transit from the endoplasmic reticulum to the cell surface. This transport is well understood from the endoplasmic reticulum to the Golgi apparatus (Saito et al, 2009; Raote & Malhotra, 2021). However, much less is known on how these BM proteins reach the cell surface and how these routes are spatiotemporally integrated in a developing tissue.

Our understanding of BM biology has been broadened by studies in invertebrates that revealed, using fluorescent tagged versions of BM components, the unexpected diversity of BM structures and dynamics (Keeley et al, 2020; Matsubayashi et al, 2020; Pastor-Pareja, 2020). Particularly, *Drosophila melanogaster* oogenesis is a highly tractable system suitable to study BM biology. The fly ovary consists of several ovarioles, each of them composed of a succession of follicles (or egg chambers) that develop up to a mature egg. This process is categorized into 14 morphologically distinct stages (Spradling et al, 1993). Each follicle comprises a germline cyst surrounded by a monolayer of somatic epithelial follicle cells. This epithelium is polarized: the apical surface faces the germline cells, whereas the basal surface is in contact with the BM that outlines each follicle (Figure 1A). All major components of this BM are synthesized and secreted by follicle cells (Isabella & Horne-Badovinac, 2015). Several factors implicated in this process have been identified. Loss of function of the small GTPases Rab10 and Rab8, or of their respective guanine nucleotide exchange factors (GEF; Crag and Stratum) leads to the mistargeting of a fraction of BM proteins towards the apical domain. This indicates that these classical cell trafficking factors are involved in BM assembly (Denef

et al, 2008; Devergne et al, 2017; Lerner et al, 2013). However, it is not known whether these factors act together or in parallel.

Importantly, the follicle BM is implicated in egg morphogenesis (Haigo & Bilder, 2011; Isabella & Horne-Badovinac, 2016). During ovarian development, the follicle progressively elongates the initial spherical shape along the antero-posterior (AP) axis from stage 3 to adopt an ovoid shape. Elongation relies on the establishment of planar cell polarity that is compulsory to launch a process of oriented collective cell migration, perpendicularly to the AP axis, from stage 1 to stage 8 of oogenesis (Haigo & Bilder, 2011). This migration causes the entire egg chamber to rotate inside the stationary extracellular matrix. This rotation allows the oriented deposition of BM fibrils, containing all BM components, onto a uniform unpolarized BM (Haigo & Bilder, 2011; Isabella & Horne-Badovinac, 2016) (Figure 2A). It was initially proposed that BM fibrils serve as a molecular corset to mechanically constrain the follicle and direct the elongation in the AP axis. However, it has been suggested that BM fibrils act as a cue for actin fiber orientation at the basal domain of follicle cells that would be the main mechanical effector of elongation (Cerqueira Campos et al, 2020). Nonetheless, BM fibrils nicely illustrate how BM diversification can elicit a morphogenetic mechanism. BM fibrils are generated from newly synthetized BM proteins that accumulate in the lateral pericellular spaces between follicular cells before being inserted in the BM into an oriented manner by the directed egg chamber rotation (Isabella & Horne-Badovinac, 2016). Rab10 overexpression leads to an increased lateral accumulation of BM proteins and of BM fibrils, suggesting its implication in the formation of these fibrils (Isabella & Horne-Badovinac, 2016). BM fibril formation requires dystroglycan (Dg), a membrane receptor for BM proteins, and dystrophin (Dys), an F-actin interacting protein (Cerqueira Campos et al, 2020). Dg and Dys are the two core components of the evolutionarily conserved dystrophin-associated protein complex (DAPC). In mutant *Dys* or *Dg* follicles, the BM is devoid of BM fibrils. Moreover, epistasis experiments with Rab10 suggest a functional link between these actors (Cerqueira Campos et al, 2020). However, how DAPC participates in BM fibril formation remains to be elucidated.

In this study, we analyzed the routes leading to BM formation in the follicular epithelium. Genetic evidence indicates that Rab8 and Rab10 define two parallel routes, forming homogenous BM and BM fibrils, respectively. Analyses of BM protein secretion in single cells revealed that this diversification is due to Rab10-driven lateral and planar polarized secretion, while Rab8 promotes basal secretion. We also found that the DAPC is part of the same cell compartment as Rab10 and influences the planar polarization of Rab10-dependent secretion. Moreover, we found that the exocyst complex is required the formation of homogenous BM.

Results

Rab8 and Rab10 are both required for BM assembly

To understand how BM is produced by the follicular epithelium, we first tested the role of the two small GTPases Rab8 and Rab10 by knocking them down (KD) using UAS RNAi transgenes induced by the follicle cell-specific driver tj:Gal4. BM assembly and secretion can be easily visualized at stage 8 of oogenesis using an endogenous GFP-tagged Col IV α2 chain, called Viking. As previously described, *Rab8* or *Rab10* KD induced the mistargeting of part of BM proteins toward the apical domain (Figure 1B-D) (Devergne et al, 2017; Lerner et al, 2013). Nonetheless, quantification of Col IV-GFP fluorescence apical pool, relative to the total secreted proteins (i.e. basal plus apical pools), indicated that in both KD most proteins were still delivered basally (Figure 1H). *Rab8* KD had a weaker effect than *Rab10* KD, as indicated by the absence of significant increase in the apical fraction compared with control. At this stage, it was unclear whether this was due to Rab8 weaker implication in BM protein secretion, redundancy with some other factor(s), or weaker *Rab8* RNAi efficiency. One attractive hypothesis was that Rab8 and Rab10, which are Rab GTPases with very similar sequences, may act in parallel. In agreement with this hypothesis, the double *Rab8-Rab10* KD completely impaired basal secretion and almost all the Col IV-GFP signal was at the apical surface (Figure 1E and H). This synergic effect of *Rab8* and *Rab10* KD suggests a partial redundancy for addressing BM proteins. Moreover, the longitudinal view of the epithelium suggested the presence of a proper basement membrane, but on the apical side. However, the planar view indicated that apically secreted BM proteins assembled in aberrant discontinuous structures, as observed in other genotypes leading to apical BM secretion (Figure S1A) (Zajac & Horne-Badovinac, 2022).

It has been previously shown that the apical secretion observed in the *Rab10* KD can be suppressed by *Rab11* KD, suggesting that Rab11 may define a cryptic route for BM protein secretion (Lerner et al, 2013). We tested this hypothesis by knocking down all three genes (*Rab8, Rab10* and *Rab11* triple KD). In this condition, apical secretion was completely blocked, and BM proteins were in big intracellular blobs (Figure 1G-H). Notably, basal secretion was not restored, indicating that Rab11 did not compete with any other route besides Rab8 and Rab10. Altogether, these data indicate that Rab8 and Rab10 define the proper path for BM secretion in a partially redundant manner, and that no other route towards the basolateral side of the follicular epithelium exists.

Considering the important role of BM in epithelial architecture, we wondered whether completely reversing BM secretion towards the apical domain (as observed in the *Rab8-Rab10* double KD) or lack of BM secretion (*Rab8, Rab10* and *Rab11* triple KD) could affect epithelial polarity. Therefore, we checked the localization of atypical protein kinase C (aPKC), an essential actor of the apical domain definition commonly used as a marker of this domain (Morais-de-Sá et al, 2010). We observed no difference between control and *Rab8-Rab10*

double KD (Figure S1B). Similarly, in the *Rab8, Rab10, Rab11* triple KD, aPKC reduction at the apical surface was not stronger than in the single *Rab11* KD, indicating that the weak defect observed in these context was independent of BM secretion impairment (Figure S1B). These data show that in the follicular epithelium, BM localization/presence has no major impact on polarity maintenance. These observations are in agreement with previous data indicating that major actors of the cell-extracellular matrix interface, such as integrins and Dg, are not required for cell polarity in the follicular epithelium (Lovegrove et al, 2019).

Rab8 and Rab10 compete to define different BM types

Findings mainly based on gain of function experiments suggest that Rab10 participates in the follicle cell BM diversification by contributing to the formation of BM fibrils that are deposited as the cells migrate (Isabella & Horne-Badovinac, 2016). On the other hand, the route to generate homogenous BM remains unknown (Figure 2A). Therefore, we analyzed the effects of Rab8 or Rab10 KD or overexpression (OE) on BM structure by assessing Col IV-GFP pattern at stage 8 (i.e. the end of BM fibril deposition). We quantified the fibril fraction (FF) that corresponds to the percentage of fluorescence detected in fibrils relative to the total BM fluorescence at the follicle basal surface. As previously observed, *Rab10* OE led to FF increase (Figures 2B, C and H). Conversely, *Rab10* KD significantly decreased FF, providing the first loss of function evidence of its involvement in BM fibril formation (Figures 2D and H). Conversely, Rab8 OE decreased the FF, whereas *Rab8* KD increased it (Figures 2E, F and H). Thus, Rab8 and Rab10 had exact opposite effects. Importantly, as in *Rab8* KD part of BM proteins was targeted to the apical surface and as the FF was relative to the total BM fluorescence at the follicle basal surface, its increase in *Rab8* KD might partly reflect a decrease of the homogenous matrix. Thus, Rab8 defines a different route than Rab10, leading ultimately to a different BM type. Previous observations indicated that a strong increase in BM fibril formation might induce a depletion of the homogenous matrix, suggesting a competition between the mechanisms promoting the two BM types (Isabella & Horne-Badovinac, 2016). We tested this hypothesis by comparing the concomitant and the single overexpression of *Rab8* and *Rab10* (combined with a *UAS*:*LacZ* transgene as a control for a potential Gal4 titration). The concomitant Rab8-Rab10 OE led to a FF value similar to control (Figures 2G and I). Altogether, these results show that Rab8 and Rab10 define two distinct routes, each responsible for a different BM type (homogenous matrix and fibrils, respectively) and in competition with each other.

Rab10 orients BM secretion towards the lateral rear cortical domain

To explain how Rab8 and Rab10 allow the formation of distinct BM types, we investigated the cell exit site of BM proteins. It has already been shown that Rab10 OE increases the lateral

secretion of BM proteins, using immunostaining against BM proteins without permeabilization (Isabella & Horne-Badovinac, 2016). However, this approach does not precisely map the exit site in single cells because it does not allow determining BM protein origin between cells and detecting any potential basal secretion. Therefore, we combined immunostaining without permeabilization with the M-TRAIL tool, initially developed to follow the migration of individual follicle cells *in vivo* (Chen et al, 2017). M-TRAIL generates single-cell clones that express a Col IV subunit protein fused to GFP, named Cg25c (UAS:Col IV-GFP). Each cell forms a fluorescent trail that corresponds to its collagen secretion while migrating (Figure 3A-B). We detected secreted Col IV with an anti-GFP antibody and a Cy3- or Cy5-conjugated secondary antibody. Expression of the UAS:Col IV-GFP transgene in the whole tissue using the follicle cell-specific driver tj:Gal4 led to the formation of a fluorescent BM, like the one observed with endogenous Col IV-GFP, indicating that the transgene was normally incorporated in the different BM types (Figure S3). Then, we analyzed Col IV-GFP secretion in single cells.

In controls (wild type), we observed that the lateral secretion occurred mostly close to the basal surface, usually at a restricted area of <1 µm high that we named sup-basal region (Figure 3C'). We could also detect some basal secretion, with foci of BM proteins at cell surface (Figure 3C''). These foci were small and did not assemble in fibrils. Importantly, since we did detect almost no signal in the lateral front region, these foci were unlikely to be due to lateral secretion that reached the basal surface and were on top of the cell while migrating. Moreover, we usually observed these foci on the back half of the cell. We developed a method to quantify these observations. Briefly, we segmented cells in 3D according to their F-actin signal. Then, we separately quantified the GFP signal at the cell cortex and basal cell surface, allowing us to determine the lateral fraction (Figure 3F). This showed that in controls, ~70% of the BM was laterally secreted (Figure 3G). We also observed that this lateral secretion was highly planar-polarized at the back of cells (Figure 3C'). We could estimate the planar polarization by calculating a vector that corresponded to the distance and orientation between the barycenter of a cylinder representing the cell wall and the lateral signal. This confirmed the robust planar polarization of the lateral secretion (Figure 3H). Altogether, these data indicated two major sites of BM secretion: one basally, and one laterally. Lateral BM secretion was predominant and highly planar-polarized.

Importantly, our approach to study BM secretion in single cells can be associated with additional UAS transgenes to overexpress genes of interest and to visualize their cell autonomous impact. This allowed us to show that *Rab10* OE in single cells strongly increased the polarized lateral fraction and depleted the basal secretion (Figure 3D and G). *Rab10* OE did not modify the planar polarization of the basal fraction (Figure 3I). We could not detect a clear effect of *Rab8* OE (Figure 3E, G, J), possibly because this transgene had a milder effect on BM (Figure 2). Nonetheless, together with the previous results, Rab10 OE effect suggests a

model in which Rab10 guides the planar polarized lateral secretion, whereas Rab8 promotes basal secretion.

Rab10 and dystrophin associate with tubular endosomes that contain BM proteins

To understand how Rab10 contributed to the lateral planar-polarized secretion of BM proteins, we compared the subcellular localization of Rab10 and of BM components. It has already been shown that Rab10 and collagen are localized at the back of follicle cells (Lerner et al, 2013). Super-resolution images, obtained with an AiryScan microscope, of endogenous tagged Rab10 (Rab10-YFP) revealed a complex distribution (Figure 4A-D). This pattern was reproduced by expression of the *UAS*:*Rab10-RFP* transgene that is easier to detect and at a temperature where this transgene has no gain of effect on FF (Cerqueira Campos et al, 2020). Moreover, this transgene allowed the concomitant observation of Col IV-GFP (Figures 4E-H and S4A-C). We observed three main localization profiles from the cell center to the basal surface. 1) At ~1-2μm from the basal cell surface, we detected big Rab10-positive vesicles, usually at the back of cells and juxtaposed to Col IV-containing vesicles (Figures 4A, E and S4A). Based on published data, this localization is close to exit sites from the Golgi apparatus (Lerner et al, 2013; Zajac & Horne-Badovinac, 2022). 2) We also observed Rab10 at the rear lateral cell cortex, mainly in the sup-basal region. This cortical localization overlapped with the area where lateral secretion occurred. Therefore, we assumed that it corresponded to the cell exit site of the Rab10 route (Figure 4B and F). 3) More basally, we detected Rab10 in a tubular compartment. Rab10 association with tubular endosomes was reported in mammalian cell culture and in *Caenorhabditis elegans* (Etoh & Fukuda, 2019; Shi et al, 2012). We detected these tubules at the back of cells. They were usually oriented in the migration axis in such way that their extremity was very close to or even reached the lateral rear of the cells (Figure 4C and G). As the tubular compartment is very close to the cell basal surface (i.e. below the z resolution of AiryScan), the presence of a very strong Col IV-GFP signal coming from the BM precluded its visualization in the intracellular basal compartment (Figure S4C). To circumvent this problem, we used two strategies. First, we looked at Col IV-GFP and Rab10-RFP expression in samples treated with collagenase before fixation (Figure S4D). Second, we performed FRAP experiments. After bleaching the Col IV-GFP signal on a large area at the surface of living follicles, we waited for 20 min to allow new cells to migrate to this area, and then acquired images of Rab10-RFP and Col IV-GFP signals at the basal surface of these cells (Figure S4E). In both approaches, we observed a partial colocalization of Col IV and Rab10 in the most basal Rab10-positive compartment. As this compartment was very close to the rear cortex of the cell where BM proteins are secreted and where Rab10 is also localized, we assumed that it corresponded to an important intermediate step of this secretory route.

Dys and Dg are both required for BM fibril formation, suggesting that they may be part of the Rab10 route (Cerqueira Campos et al, 2020). To better understand their contribution, we

knocked in superfolder GFP (sfGFP) at the C-terminus of Dys to label all known isoforms produced by the *Dys* locus. Dys-sfGFP was enriched at the basal surface of follicular cells and its localization was strongly planar-polarized at all the stages of follicle rotation with an enrichment at the back of cells (Figure 4I-J). Super-resolution images revealed that Dys drew parallel filaments at the basal domain that extended to approximatively half of the cells at stage 8 and showed a strong colocalization with actin stress fibers (Figure 4I). Dys was also localized at the lateral back cortex in the sup-basal region (Figure 4K). It also strongly colocalized, though not perfectly, with Rab10, both at cell cortex and at the tubular compartment (Figure 4J-K). Altogether, these data identified Dys and Rab10 as part of a highly planar polarized subcellular compartment, with structures reminiscent of tubular endosomes. This compartment contained BM proteins and was oriented towards the BM protein cell exit site, suggesting that Rab10 and the DAPC act together to regulate their lateral secretion.

DAPC is sufficient to recruit and redirect the Rab10-dependent secretory route

To investigate DAPC involvement in the Rab10 route, we analyzed their functional relationship. We previously showed that Rab10 overexpression can rescue FF in follicle cells in which *Dys* was knocked down by RNAi, suggesting that DAPC function in BM fibrils might be accessory (Cerqueira Campos et al, 2020). However, when we overexpressed *Rab10* in a *Dys* null mutant, FF was not rescued, indicating that Dys presence is obligatory for BM fibril formation (Figures 5A, B, E). Nonetheless, the absence of BM protein apical secretion in the *Dys* mutants indicated that they behaved differently than a Rab10 loss of function (Figures 5F, J).

We hypothesized that DAPC recruits vesicles containing BM proteins for the Rab10 route and that in its absence, all BM proteins use the Rab8-dependent route, leading to the exclusive formation of homogenous BM. In this scenario, *Dys* loss should completely suppress the apical secretion observed in Rab10 KD cells and block BM formation in the absence of Rab8. As apical secretion was not suppressed in *Dys* null mutant follicles upon *Rab10* KD, we excluded this hypothesis (Figures 5F, G, J). However, apical secretion was strongly increased in *Dys* null mutant follicles upon *Rab8* KD, although it was not sufficient to block basal BM formation. We interpret this result as the consequence of the competition between the Rab8 and Rab10 routes in a genetic context where the Rab10 route is affected, ultimately leading to more BM proteins transported by the Rab8 route. Moreover, in this genetic combination (*Dys* null mutant + *Rab8* KD) there is no FF rescue (Figures 5D-E). Thus, in the absence of Dys, a significant fraction of BM proteins still used the Rab10 route, but did not generate fibrils. Next, we asked whether Dys could regulate the subcellular targeting of the Rab10 route. In *Dys* null mutant clones we did not observe any change in Rab10-RFP localization compared with the neighboring wild type cells (Figure S5A). We then quantified Rab10 polarized localization at the cell cortex by calculating the mean signal intensity ratio between the boundaries

corresponding to the trailing edge of the follicle cell and those parallel to the migration axis. We did not find any difference (Figure S5B). We analyzed BM secretion at single-cell resolution in *Dys* null mutant cells and did not detect any significant difference in the ratio between lateral and basal secretions and in the planar polarization of the lateral secretion (Figure S5C-D).

To better understand the relationship between DAPC and Rab10, we also induced *Dg* OE in the follicular epithelium. Although the precise localization of endogenous Dg is unknown, when overexpressed, the protein localized at the basal surface and also all along the lateral and apical cortex of follicle cells (Figure 5K and Figure S5E). We think that this Dg localization was ectopic and due to its overexpression. Indeed, it induced the recruitment of Dys-sfGFP to the whole cell periphery where Dys is normally absent, and depleted Dys from the basal tubular compartment (Figure 5L and Figure S5F-G). Consequently, Dys cortical localization was no more planar-polarized (Figure 5L' and P). Strikingly, Dg OE led to Rab10 recruitment to the whole lateral cortex, abolishing its planar polarization. This suggested a physical link between the DAPC and Rab10 (Figures 5M and Q). As Dys is required for BM fibril formation, such Rab10 recruitment upon Dg OE might be related to BM fibril formation, and is likely to be Dys-dependent. We tested this hypothesis by overexpressing *Dg* in a *Dys* null mutant background. In this context, Rab10 was not recruited to the lateral cortex and was still planar polarized, whereas Dg was still located at the whole cell periphery (Figures 5N, O, Q and Figure S5H-I). Thus, Dys is required for Rab10 recruitment by Dg.

Interestingly, Rab10 delocalization induced by Dg OE allowed us to test specifically the role of the planar-polarized lateral secretion versus unpolarized secretion from the whole lateral periphery. We analyzed BM protein secretion in Dg OE follicle cells. FF quantification revealed a slight increase following Dg OE (Figure S5J-L). However, probably as a direct consequence of Rab10 redistribution all around the cells, we noticed the presence of very long and intense fibrils that remained trapped between the lateral domain of the follicle cells in the axis of cell migration (Figure 5S, S5L?). As recently reported in another genetic context affecting BM secretion routes and where similar lateral fibrils were described, their presence disrupted the cell geometry (Figure 5R-S and (Zajac & Horne-Badovinac, 2022)). Altogether, these data underly that BM protein secretion planar polarization is required to maintain the epithelial structure. They also show that Dg is sufficient to reorient the Rab10 route.

<u>Exo70 interacts with and limits dystrophin planar polarization</u>

To understand how Rab10 and the DAPC could be connected, we noticed that the exocyst subunit Exo70 was identified as a Dys interactor using a large scale two-hybrid proteomic approach (Formstecher et al, 2005). Exocyst is an octameric complex, very conserved from yeast to humans. It is usually involved in the subcellular targeting of exocytosis by tethering vesicles to a specific location on the plasma membrane, but it can also participate in vesicle

transport or docking (Nishida-Fukuda, 2019; Wu & Guo, 2015). A physical interaction between Dys and the exocyst complex could be likely because this complex has been functionally linked with Dys and Rab10 in other contexts (Naegeli et al, 2017; Yatsenko et al, 2021; Chen et al, 2014; Taylor et al, 2015; Zou et al, 2015). Although yeast two-hybrid approaches may generate false positives, mining of initial data indicated that multiple overlapping fragments of Dys were identified in a screen with fly Exo70 as prey, strongly increasing the confidence (Figure 6A). Dys long isoforms include an actinin domain that can bind to F-actin, a long rod domain that contains spectrin repeats (SR), and a C-terminal domain that includes the Dg binding region. The minimal interaction domain with Exo70, deduced from the yeast two-hybrid results, overlapped with two SRs that corresponded to amino acids 2549-2635 on the longest fly Dys isoform (RH). Based on their position and homology, these two SRs correspond to SR22 and SR23 in mammalian dystrophin (Figure 6A). The interacting domain also corresponded to the most conserved part of the whole rod domain from fly to humans (53% and 70% of amino acid identity and homology, respectively). However, no clear function or protein interaction has been assigned to it yet. GST pull-down experiments with a Dys SR22-SR23-containing fragment and Exo70 confirmed their direct interaction (Figure 6B). Overexpressed Exo70 fused to the Scarlet fluorescent protein localized to the whole cell cortex (Figures 6D, H). Exo70 OE led to Dys recruitment (Figure 6C-D) and reduced Dys cortical planar polarity *in vivo* (Figure 6F). However, unlike Dg OE that recruits both Dys and Rab10, Exo70 OE did not affect Rab10 polarized localization (Figures 6G, H and J). Altogether, these data indicate that Dys and Exo70 interact directly. They also suggest that this interaction is not implicated in the DAPC-Rab10 interaction, and consequently exocyst may not provide a link between them.

In *Exo70* null mutant follicles, Dys localization was hyperpolarized in the sup-basal region with a stronger signal at the rear cell cortex, the opposite of what observed in Exo70 OE (Figure 6E-F). We also observed a stronger Rab10 localization in the same domain in *Exo70* null mutants, although the effect was less obvious than for Dys (Figure 6I-J). Thus, Exo70 limits Dys planar polarization and consequently that of Rab10, confirming that Dys-Exo70 interaction does not provide a link between Rab10 and Dys.

To uncover a potential role of Dys-Exo70 interaction, we analyzed exocyst involvement in BM formation. In *Exo70* null mutants, which are viable, FF was strongly increased (Figure 6L,N and P). We reproduced this defect by inducing, in the follicular epithelium, RNAi against *Exo70* and also against the other seven subunits of the exocyst complex (Figure S6A). Moreover, we confirmed that in the *Exo70* null mutant, the BM defect could be rescued by Exo70 OE in follicle cells (Figure S6B-E).

The *Exo70* null mutant impact on BM is consistent with Dys and Rab10 hyperpolarization. As exocyst and Dys loss of function show opposite effects on BM, we could perform an epistasis test. We did not manage to recover double *Dys* and *Exo70* null mutant flies, therefore we induced *Exo70* KD in follicle cells in a *Dys* null mutant background. The FF decrease to the level

observed in the *Dys* mutant clearly indicated that *Dys* was epistatic to *Exo70* (Figures 6M, O, P). This finding favored a model in which Exo70 limits BM fibril formation by modulating Dys localization.

Exocyst is required for the Rab8-dependent route

We also analyzed the effect of the *Exo70* null mutant on BM secretion at the single-cell level. Lateral secretion was still oriented towards the back of the cells, consistently with the fact that the Dys-Rab10 route was still planar polarized (Figure 7A-B). Conversely, the basal secretion was strongly impaired with almost no BM protein detected at the basal surface of Col IV-GFP expressing cells (Figure 7A and C). Therefore, we asked whether Exo70 may interfere with BM formation by an additional way than Dys hyperpolarization, and whether this could influence the Rab8 route. Three hypotheses could explain the *Exo70* phenotype: 1) the Rab8 route is mistargeted towards the lateral domain to make BM fibrils like in the Rab10 route; 2) all BM proteins are directed towards the Rab10 route; 3) the Rab8 route is blocked and cannot induce basal secretion. If the Rab8 route were mistargeted, then Rab8 loss, which normally increases FF, should decrease FF in the *Exo70* loss of function context. However, we did not observe any FF change in WT and *Exo70* KD follicles upon *Rab8* KD. This ruled out the first hypothesis (Figure 7D). If all BM proteins were taken in charge by the Rab10 route in the *Exo70* null mutant, then Rab10 overexpression should not enhance the impact on FF. However, Rab10 OE in the *Exo70* null mutant background strongly increased FF, which tends to exclude the second hypothesis (Figure 7D).

If the Rab8 route were blocked, then concomitantly blocking the Rab10 route should completely inhibit basolateral secretion. Strikingly, in the *Rab10* and *Exo70* double KD, we could not detect Col IV-GFP at the basal surface of the follicular epithelium (Figure 7E-H). However, in such condition there is almost no apical secretion, compared for instance to the *Rab10* and *Rab8* double KD (Figure 1), suggesting a complete inhibition of the routes for BM formation. Also, we never observed apical secretion in *Exo70* KD follicles (Figure 7E), indicating that *Exo70* KD effect was different compared with that of *Rab8* KD. Together, these results suggest that Exo70 is required for the Rab8-dependent BM route and at least to some extent, for the Rab11 cryptic route.

Lastly, we checked whether Exo70 effect on the Rab8 route was independent of its effect on Dys localization. As previously shown, in the *Rab10-Exo70* double KD, there was no basolateral secretion, excluding the hypothesis that Exo70 acts exclusively through hyperpolarization of the Rab10 route (Figure 7G). Conversely, *Rab8 KD* did not affect Dys localization unlike the *Exo70* null mutant (Figure 7I). These results tend to confirm that Exo70 participates in follicle BM secretion via two independent mechanisms.

Discussion

Proper BM protein secretion and BM diversification are essential for development. Our work brings new mechanistic insights into how BM proteins are secreted in epithelial cells and demonstrates that BM diversification during development can arise from the existence of different secretory routes with different cell exit sites.

Strikingly, these routes are highly integrated in the different polarity axes (i.e. apical basal cell polarity and planar cell polarity). First, our results indicate that Rab8 targets a route towards the basal domain, although our data on its effect at the single-cell level are not conclusive. However, the absence or strong reduction of basal secretion in the *Exo70* null mutant and *Rab10* OE conditions provides evidence for such a basal targeting. Second, we provide evidence that the Rab10 route is laterally targeted, although close to the basal surface at the sup-basal region, and planar-polarized towards the rear of cells. Third, as previously proposed, our data confirm the existence of a cryptic route towards the apical surface via Rab11 (Lerner et al, 2013). Thus, three different Rab proteins are targeted towards the three distinct domains of epithelial cells defined by apical basal polarity, and at least of them is also planar polarized. These three Rab GTPases have been jointly involved in different processes (Knödler et al, 2010; Sato et al, 2014; Vogel et al, 2015; Eguchi et al, 2018; Häsler et al, 2020). However, these observations mainly came from mammalian cell culture systems with unpolarized cells or from pathological situations where apical basal polarity was disrupted. Here, these routes could be considered as partially redundant because they are all involved in BM protein secretion and all three must be knocked down to completely block it. However, the integration of these routes to cell polarity clearly allowed distinguishing the spatial specificity of these three Rab proteins and revealed that they compete with each other.

The next obvious question is how these routes are differentially integrated with cell polarity. Part of the answer likely comes from microtubule-associated transport, and two kinesins, Khc-73 and Khc, involved in the basolateral targeting of BM-containing vesicles (Zajac & Horne-Badovinac, 2022). Their concomitant loss of function phenocopies, to some extent, the double *Rab8-Rab10* KD, suggesting that both routes of BM protein basolateral secretion are affected when these kinesins are absent. While a direct link between Rab10 and the Khc-73 homolog has been established, one could speculate that Kin1 activity might be more related to the Rab8 route (Etoh & Fukuda, 2019). Nonetheless, our data indicate that microtubule transport is not the only difference between these routes.

We established a functional link between the exocyst complex and Rab8. This link has been shown in other systems, including BM remodeling, suggesting that it might be a general feature of the Rab8-dependent route (Das & Guo, 2011; Feng et al, 2012; Mavor et al, 2016; Bravo-Cordero et al, 2007; Monteiro et al, 2013). However, we showed, for the first time, the involvement of exocyst in BM secretion. Importantly, the absence of basal secretion in *Exo70*

mutants and the genetic evidence of Exo70 requirement for the Rab8 route confirm that the Rab8 route is targeted towards the basal domain of the cells.

Moreover, several of our results are in favor of a direct involvement of Dys and Dg in the Rab10 route. First, Dys is highly associated with the Rab10 compartment, and DAPC is required for BM fibril formation. Second, in the absence of Dys, BM protein diversion towards the apical domain is increased upon Rab8 KD. This result excludes a model in which Dys participates in BM fibril formation only after BM protein secretion. Moreover, we showed that Dg distribution all around the cells, when overexpressed, is sufficient to redistribute Rab10 and to induce aberrant BM secretion, confirming a functional link. However, we could not detect any alteration in Rab10 localization and collagen lateral secretion in the absence of Dys. Therefore, more investigations are required to define exactly how the DAPC allows the formation of BM fibrils. Nonetheless, given the importance of the DAPC and BM proteins in muscular dystrophies, our results will pave the way to determine whether a similar function is present also in muscle cells. Interestingly, the extracellular matrix is different between the myotendinous junction and the interjunctional sarcolemmal basement membrane and may provide another developmental context where several routes targeted to different subcellular domains may be implicated.

Lastly, we revealed another level of regulation of this process based on the direct interaction between Dys and Exo70 to modulate Dys localization. Functional links have been proposed between the exocyst complex and Dg, but they had never been associated through a direct molecular link and Dys involvement was not shown (Naegeli et al, 2017; Yatsenko et al, 2021). The high conservation of the interaction domain on Dys, a domain with no other known interacting protein, suggests that this interaction has been conserved during evolution and may be relevant in other contexts.

Our work identified distinct actors of the Rab8- and Rab10-dependent routes for BM protein secretion, with the involvement of the DAPC and exocyst complexes. However, more studies are required to understand the underpinnings of such specificity between these very close Rab GTPases. The fact that Rab8 and Rab10 share a similar function (BM protein secretion), but with a different output (homogenous vs fibrillar BM), in a highly tractable system for genetics and imaging, offers a unique opportunity to thoroughly investigate their molecular and mechanistic specificities. On the basis of the present results, we propose the co-existence of parallel secretory routes orchestrated by these Rab proteins with different cell exit sites defined by cell polarity axes as the basic mechanism to explain BM diversification during development.

EXPERIMENTAL PROCEDURES

Genetics

All the fly strains used are described in Table S1 The detailed final genotypes, temperature and heat-shock conditions are given in Table S2.

Dissection and immunostaining

Resources and reagents are listed in Table S1. Ovaries were dissected in supplemented Schneider medium, ovarioles were separated and the muscle sheath was removed before fixation to obtain undistorted follicles. Ovaries were fixed with 4% paraformaldehyde in PBS containing phalloidin Atto-488, phalloidin Atto-550 or phalloidin Atto-633 (Sigma) for 20 min, washed 3 times in PBS, and permeabilized with 0.02% Triton X-100 containing phalloidin Atto-488, -550 or -633 to stain F-actin. For antibody staining, dissected ovaries were fixed with 4% formaldehyde in PBS containing phalloidin Atto-488, phalloidin Atto-550 or phalloidin Atto-633 (Sigma) for 15 min. After blocking and permeabilization with PBS, 0.5% BSA and 0.2% Triton X-100 (PBT), primary antibodies were diluted in PBT and detected with Alexa Fluor-conjugated secondary antibodies. Antibodies are described in Table S1. F-actin was labeled with phalloidin Atto-488, -550 or -633. For non-permeabilized experiments, the anti-GFP antibody to detect pericellular BM was used as described above using PBS, 0.5% BSA (PBS-BSA) instead of PBT. For collagenase treatment, dissected ovarioles were incubated in 100µl supplemented Schneider medium containing 165 U of collagenase for 10 min followed by three washes in supplemented Schneider medium before fixation with 4% paraformaldehyde in PBS, phalloidin Atto-633, 2for 0 min. Images were taken using a Leica SP8 (for fibril fraction determination) or a Zeiss LSM800 Airyscan or a Zeiss LSM960 Airyscan2 confocal microscope.

Cloning and transgenesis

Scarlet and Exo70 cDNAs were cloned in frame in pUASz using the EBuilder HiFi DNA Assembly Cloning Kit. Site-directed transgenesis was performed at the attP40 site. The sequence corresponding to the Dys spectrin repeats 22-23 (amino acids 2549-2636 of the DysPH isoform) were cloned in frame in the pGex4T3.1. The Dys::sfGFP knock-in line was generated by the inDroso Functional Genomics (Rennes, France) using the following strategy. After cleavage with a gRNA (GACGACGACCACGGCAACCA CGG), a cassette that contained the Dys coding sequence end in frame with sfGFP and a selection marker between the LoxP sites was introduced by recombination. After obtaining the transgenic line, the selection marker was removed by crosses with a CreLox line.

GST pull-down experiments

GST and GST-DysSR22-23 were produced in BL21 bacteria using a standard protocol and were purified on Glutathione Sepharose 4B (GE Healthcare). Exo70 was produced by *in vitro* transcription and translation in the presence of S^{35} using standard protocols. Interactions were tested in 50mM Tris HCl, 100mM NaCl, 0.01%Triton-X100, 0.1% BSA at 20°C for 12 hours before washes in 50mM Tris HCl, 100mM NaCl, 0.01%Triton.

BM fibril fraction and BM apical fraction

BM fibril fraction (FF) was determined using a homemade Fiji macro, as previously described (Cerqueira Campos et al, 2020). The BM apical fraction was quantified using the Fiji tool to measure and compare the 'mean gray value' of pairs of regions of interest (ROIs) drawn alongside the cell apical and basal walls (about 25 ROI pairs for each genotype, 3 to 13 cells).

Dg, Dys and Rab10 trailing vs lateral signal intensity ratio

The Fiji freehand line tool was used to manually trace two lines per follicle cell, following the F-actin signal: one line on the trailing edge and the other one along one of the two lateral sides of the cell, on a projection of three focal plans with a Z step of 0.15 µm starting at ~0.15 µm away from the basal surface. A third line, drawn away from the F-actin signal, was used for background subtraction. The 'mean gray values' for Dg, Dys, and Rab10 signal were determined and the lateral signal fraction was plotted.

BM protein secretion quantification

Follicle cells were manually segmented based on F-actin signal, on nine successive focal plans with a Z step of 0.15 µm, from the basal surface (detected as the Z focal plan giving the best signal for actin stress fibers) towards the apical surface. BM protein secretion was quantified using a homemade Fiji macro to detect the signal intensity given by anti-GFP antibody immunostaining without permeabilization in single-cell clones that express UAS:Col IV-GFP. The lateral secretion orientation was assessed by determining the position of the barycenter of the hollow cylinder of 1.5 µm thickness to model the nine ROIs. The signal intensity and direction, defined by the vector between the isobarycenter of the cylinder and its center of mass, was measured using the signal intensity as weight. The basal secretion was assessed by measuring the signal intensity of a full cylinder made by projecting the ROI drawn on the basal surface, and shrunk to 0.75 µm in diameter, on the three slices beyond the cell surface. The fraction of laterally secreted BM proteins was determined as the percentage of signal intensity from the lateral secretion relative to the total signal intensity measured from the two cylinders. A ROI drawn on non-GFP cells and reported on the same nine lateral Z focal plans

and three slices beyond basal surface was used to subtract the background lateral and basal signals.

Statistical analyses

For all experiments, the minimum sample size is indicated in the figure legends. Results were obtained from at least two independent experiments, and for each experiment multiple females were dissected. Randomization or blinding was not performed. Data normality was calculated using the D'Agostino and Pearson normality test. The unpaired t-test was used to compare samples with normal distribution, and the unpaired Mann– Whitney test for samples without normal distribution. Graphs were generated with Prism.

Acknowledgements

We are grateful to M.-L. Parmentier and V. Van De Bor for sharing fly stocks. This work was supported by the Association Française contre les Myopathies (AFM) (Trampoline grant 17683 and MyoNeurAlp network). This research was also financed by the French government IDEX-ISITE initiative 16-IDEX-0001 (CAP 20-25). We also thank the CLIC facility (Clermont Imagerie Confocale).

References

Bonnans C, Chou J, Werb Z (2014) Remodelling the extracellular matrix in development and disease. *Nat Rev Mol Cell Biol* **15**.
Bravo-Cordero JJ, Marrero-Diaz R, Megías D, Genís L, García-Grande A, García MA, Arroyo AG, Montoya MC (2007) MT1-MMP proinvasive activity is regulated by a novel Rab8-dependent exocytic pathway. *EMBO J* **26**.
Cerqueira Campos F, Dennis C, Alégot H, Fritsch C, Isabella A, Pouchin P, Bardot O, Horne-Badovinac S, Mirouse V (2020) Oriented basement membrane fibrils provide a memory for F-actin planar polarization via the Dystrophin-Dystroglycan complex during tissue elongation. *Development* **147**.
Chaudhuri O, Cooper-White J, Janmey PA, Mooney DJ, Shenoy VB (2020) Effects of extracellular matrix viscoelasticity on cellular behaviour. *Nature* **584**.
Chen DY, Crest J, Bilder D (2017) A Cell Migration Tracking Tool Supports Coupling of Tissue Rotation to Elongation. *Cell Rep* **21**: 559-569.
Chen S, Li L, Li J, Liu B, Zhu X, Zheng L, Zhang R, Xu T (2014) SEC-10 and RAB-10 coordinate basolateral recycling of clathrin-independent cargo through endosomal tubules in Caenorhabditis elegans. *Proc Natl Acad Sci U S A* **111**.
DAC W, Yamada KM (2020) The extracellular matrix in development. *Development* **147**.
Das A, Guo W (2011) Rabs and the exocyst in ciliogenesis, tubulogenesis and beyond. *Trends Cell Biol* **21**.
Denef N, Chen Y, Weeks SD, Barcelo G, Schüpbach T (2008) Crag regulates epithelial architecture and polarized deposition of basement membrane proteins in Drosophila. *Dev Cell* **14**: 354-364.
Devergne O, Sun GH, Schüpbach T (2017) Stratum, a Homolog of the Human GEF Mss4, Partnered with Rab8, Controls the Basal Restriction of Basement Membrane Proteins in Epithelial Cells. *Cell Rep* **18**: 1831-1839.
Eguchi T, Kuwahara T, Sakurai M, Komori T, Fujimoto T, Ito G, Yoshimura SI, Harada A, Fukuda M, Koike M, Iwatsubo T (2018) LRRK2 and its substrate Rab GTPases are sequentially targeted onto stressed lysosomes and maintain their homeostasis. *Proc Natl Acad Sci U S A* **115**.
Etoh K, Fukuda M (2019) Rab10 regulates tubular endosome formation through KIF13A and KIF13B motors. *J Cell Sci* **132**.
Feng S, Knödler A, Ren J, Zhang J, Zhang X, Hong Y, Huang S, Peränen J, Guo W (2012) A Rab8 guanine nucleotide exchange factor-effector interaction network regulates primary ciliogenesis. *J Biol Chem* **287**.
Formstecher E, Aresta S, Collura V, Hamburger A, Meil A, Trehin A, Reverdy C, Betin V, Maire S, Brun C, Jacq B, Arpin M, Bellaiche Y, Bellusci S, Benaroch P, Bornens M, Chanet R, Chavrier P, Delattre O, Doye V, Fehon R, Faye G, Galli T, Girault JA, Goud B, de Gunzburg J, Johannes L, Junier MP, Mirouse V, Mukherjee A, Papadopoulo D, Perez F, Plessis A, Rossé C, Saule S, Stoppa-Lyonnet D, Vincent A, White M, Legrain P, Wojcik J, Camonis J, Daviet L (2005) Protein interaction mapping: a Drosophila case study. *Genome Res* **15**: 376-384.
Haigo SL, Bilder D (2011) Global Tissue Revolutions in a Morphogenetic Movement Controlling Elongation. *Science* **331**: 1071-1074.
Häsler SLA, Vallis Y, Pasche M, McMahon HT (2020) GRAF2, WDR44, and MICAL1 mediate Rab8/10/11-dependent export of E-cadherin, MMP14, and CFTR ΔF508. *J Cell Biol* **219**.
Humphrey JD, Dufresne ER, Schwartz MA (2014) Mechanotransduction and extracellular matrix homeostasis. *Nat Rev Mol Cell Biol* **15**.

Isabella AJ, Horne-Badovinac S (2015) Building from the Ground up: Basement Membranes in Drosophila Development. *Curr Top Membr* **76**: 305-336.
Isabella AJ, Horne-Badovinac S (2016) Rab10-Mediated Secretion Synergizes with Tissue Movement to Build a Polarized Basement Membrane Architecture for Organ Morphogenesis. *Dev Cell* **38**: 47-60.
Jayadev R, Sherwood DR (2017) Basement membranes. *Curr Biol* **27**.
Keeley DP, Hastie E, Jayadev R, Kelley LC, Chi Q, Payne SG, Jeger JL, Hoffman BD, Sherwood DR (2020) Comprehensive Endogenous Tagging of Basement Membrane Components Reveals Dynamic Movement within the Matrix Scaffolding. *Dev Cell* **54**.
Knödler A, Feng S, Zhang J, Zhang X, Das A, Peränen J, Guo W (2010) Coordination of Rab8 and Rab11 in primary ciliogenesis. *Proc Natl Acad Sci U S A* **107**.
Kyprianou C, Christodoulou N, Hamilton RS, Nahaboo W, Boomgaard DS, Amadei G, Migeotte I, Zernicka-Goetz M (2020) Basement membrane remodelling regulates mouse embryogenesis. *Nature* **582**.
Lerner DW, McCoy D, Isabella AJ, Mahowald AP, Gerlach GF, Chaudhry TA, Horne-Badovinac S (2013) A Rab10-Dependent Mechanism for Polarized Basement Membrane Secretion during Organ Morphogenesis. *Dev Cell* **24**: 159-168.
Lovegrove HE, Bergstralh DT, D SJ (2019) The role of integrins in Drosophila egg chamber morphogenesis. *Development* **146**.
Matsubayashi Y, Sánchez-Sánchez BJ, Marcotti S, Serna-Morales E, Dragu A, Díaz-de-la-Loza MD, Vizcay-Barrena G, Fleck RA, Stramer BM (2020) Rapid Homeostatic Turnover of Embryonic ECM during Tissue Morphogenesis. *Dev Cell* **54**.
Mavor LM, Miao H, Zuo Z, Holly RM, Xie Y, Loerke D, Blankenship JT (2016) Rab8 directs furrow ingression and membrane addition during epithelial formation in Drosophila melanogaster. *Development* **143**.
Monteiro P, Rossé C, Castro-Castro A, Irondelle M, Lagoutte E, Paul-Gilloteaux P, Desnos C, Formstecher E, Darchen F, Perrais D, Gautreau A, Hertzog M, Chavrier P (2013) Endosomal WASH and exocyst complexes control exocytosis of MT1-MMP at invadopodia. *J Cell Biol* **203**.
Morais-de-Sá E, Mirouse V, St Johnston D (2010) aPKC phosphorylation of Bazooka defines the apical/lateral border in Drosophila epithelial cells. *Cell* **141**: 509-523.
Mouw JK, Ou G, Weaver VM (2014) Extracellular matrix assembly: a multiscale deconstruction. *Nat Rev Mol Cell Biol* **15**.
Munjal A, Hannezo E, Tsai TY, Mitchison TJ, Megason SG (2021) Extracellular hyaluronate pressure shaped by cellular tethers drives tissue morphogenesis. *Cell* **184**.
Naegeli KM, Hastie E, Garde A, Wang Z, Keeley DP, Gordon KL, Pani AM, Kelley LC, Morrissey MA, Chi Q, Goldstein B, Sherwood DR (2017) Cell Invasion In Vivo via Rapid Exocytosis of a Transient Lysosome-Derived Membrane Domain. *Dev Cell* **43**: 403-417.e10.
Nishida-Fukuda H (2019) The Exocyst: Dynamic Machine or Static Tethering Complex? *Bioessays* **41**.
Palmquist KH, Tiemann SF, Ezzeddine FL, Yang S, Pfeifer CR, Erzberger A, Rodrigues AR, Shyer AE (2022) Reciprocal cell-ECM dynamics generate supracellular fluidity underlying spontaneous follicle patterning. *Cell* **185**.
Pastor-Pareja JC (2020) Atypical basement membranes and basement membrane diversity - what is normal anyway? *J Cell Sci* **133**.
Raote I, Malhotra V (2021) Tunnels for Protein Export from the Endoplasmic Reticulum. *Annual review of biochemistry* **90**.

Saito K, Chen M, Bard F, Chen S, Zhou H, Woodley D, Polischuk R, Schekman R, Malhotra V (2009) TANGO1 facilitates cargo loading at endoplasmic reticulum exit sites. *Cell* **136**.
Sato T, Iwano T, Kunii M, Matsuda S, Mizuguchi R, Jung Y, Hagiwara H, Yoshihara Y, Yuzaki M, Harada R, Harada A (2014) Rab8a and Rab8b are essential for several apical transport pathways but insufficient for ciliogenesis. *J Cell Sci* **127**.
Sherwood DR (2021) Basement membrane remodeling guides cell migration and cell morphogenesis during development. *Curr Opin Cell Biol* **72**.
Shi A, Liu O, Koenig S, Banerjee R, Chen CC, Eimer S, Grant BD (2012) RAB-10-GTPase-mediated regulation of endosomal phosphatidylinositol-4,5-bisphosphate. *Proc Natl Acad Sci U S A* **109**.
Spradling AC, Bate M, Arias AM (1993) The development of Drosophila melanogaster. *The Development of Drosophila Melanogaster* **1**: 1-70.
Taylor CA, Yan J, Howell AS, Dong X, Shen K (2015) RAB-10 Regulates Dendritic Branching by Balancing Dendritic Transport. *PLoS Genet* **11**.
Tiainen M, Ylikorkala A, Makela TP (1999) Growth suppression by Lkb1 is mediated by a G(1) cell cycle arrest. *Proc Natl Acad Sci U S A* **96**: 9248-9251.
Vogel GF, Klee KM, Janecke AR, Müller T, Hess MW, Huber LA (2015) Cargo-selective apical exocytosis in epithelial cells is conducted by Myo5B, Slp4a, Vamp7, and Syntaxin 3. *J Cell Biol* **211**.
Wu B, Guo W (2015) The Exocyst at a Glance. *J Cell Sci* **128**.
Yatsenko AS, Kucherenko MM, Xie Y, Urlaub H, Shcherbata HR (2021) Exocyst-mediated membrane trafficking of the lissencephaly-associated ECM receptor dystroglycan is required for proper brain compartmentalization. *Elife* **10**.
Zajac AL, Horne-Badovinac S (2022) Kinesin-directed secretion of basement membrane proteins to a subdomain of the basolateral surface in Drosophila epithelial cells. *Curr Biol* **32**.
Zou W, Yadav S, DeVault L, Nung Jan Y, Sherwood DR (2015) RAB-10-Dependent Membrane Transport Is Required for Dendrite Arborization. *PLoS Genet* **11**: e1005484.

FIGURE LEGENDS

Figure 1: Rab8 and Rab10 are both required for BM assembly

(A) Scheme of a stage 8 ovarian follicle; zoom of the boxed region highlights the apical-basal axis of the follicle cell epithelium (BM, basement membrane; Ant, Anterior; Post, posterior). This scheme and all images are oriented according to the anteroposterior axis. (B-G) Cross-sections of stage 8 ovarian follicles showing Col IV-GFP (green, top; white, bottom) and F-actin (magenta) expression/localization in the following genotypes: (B) *tj:Gal4* (control), (C) *tj>Rab8* RNAi *(*Rab8 knock-down (KD)), (D) *tj>Rab10* KD, (E) *tj>Rab8>Rab10* double KD, f(F) *tj>Rab11* KD, (G) t*j>Rab8>Rab10>Rab11* triple KD. Scale bar, 10 µm. (H) Apical fraction quantification (%) of Col IV-GFP fluorescence intensity in stage 8 follicles of the indicated genotypes. Data are the mean ± SD; **p <0.01, ****p <0.0001 (one-way ANOVA with Kruskal-Wallis comparisons test); n = 13, 7, 8, 6, 7, 7 follicles (for the genotypes shown on the graph).

Figure 2: Rab8 and Rab10 compete to define two BM types

(A) Schemes of stage 3 (left) and stage 8 (right) ovarian follicles with the corresponding BM type (bottom). The pink arrow indicates the collective cell migration axis. (B-G) Basal view of the BM (Col IV-GFP*)* at stage 8 in (B) *tj:Gal4,* (Control), (C) *tj>Rab10-RFP (Rab10 overexpression (OE))*, (D) *tj>Rab10* RNAi (knock-down (KD)), (E) *tj>Rab8-YFP*, (F) *tj> Rab8* KD, (G) double *tj, >Rab10-RFP>Rab8-YFP*. Scale bars, 10 µm. (H) Quantifications of BM fibril fraction (%) in stage 8 follicles of the indicated genotypes (n = 32, 22, 12, 23, 11 follicles). (I) Quantifications of BM fibril fraction (%) in stage 8 *Col IV-GFP*-expressing follicles of the following genotypes: *tj >LacZ OE, tj>LacZ>Rab8-YFP* double *OE, tj >LacZ>Rab10-RFP* double *OE, tj>Rab8-YFP>Rab10-RFP double OE*. Data are the mean ± SD. *p <0.05, ***p <0.01, ****p <0.0001 (one-way ANOVA with Kruskal-Wallis comparisons test). In order on the graph, n = 21, 25, 23, 24 follicles.

Figure 3: BM proteins are secreted from two distinct subcellular domains

(A) Scheme of the genetic components used to generate single-cell clones that overexpress Col IV-GFP and the protein of interest. (B) Image of a whole stage 8 follicle after induction of Col IV-GFP expression (green) in single-cell clones stained for F-actin (red) and GFP (yellow) without permeabilization to label secreted Col-IV-GFP. (C-E) lateral (C-E’) and basal (C’’-E’’) focal planes of individual single-cell clones of the indicated genotypes expressing Col IV-GFP (green, top) and stained for F-actin (magenta) and GFP (white). Color-coded z projection in function of the z axis of the lateral and basal focal planes used for BM secretion quantifications (C’’’-E’’’). Scale bars, 5 µm. (F) Scheme of how BM secretion was quantified: lateral secretion was assessed using a hollow cylinder (green) of 1.5µm thickness based on cell cortex segmentation. Basal secretion was assessed using a full cylinder (red) made by projecting the ROI drawn on the basal surface and shrunk to 0.75µm in diameter on the three slices beyond

the cell surface. (G) Quantification of the lateral fraction of BM secretion (%) in single-cell clones of the indicated genotypes overexpressing Col IV-GFP. In order on the graph, n= 21, 29, and 18 cells. Data are the mean ± SD; **p <0.01 (one-way ANOVA). (H-J) Quantification of the planar orientation of lateral BM protein secretion from individual single-cell clones of the following genotypes: control (red), Rab10 OE (green), Rab8 OE (blue). Each arrow represents the vector between the isobarycenter of the hollow cylinder and its center of mass for one cell, using the signal intensity as weight. Images were oriented in such a way that the cell back points toward -90°.

Figure 4: Rab10 associates with tubular structures containing BM proteins

(A-H) Basal (C,G), sup-basal (i.e. 0.4 µm above basal surface) (B, F), and middle (i.e. 0.8 µm above basal surface) (C, G) views or color-coded z projections as a function of the z axis starting from the basal surface (D, H) of stage 8 follicles that express endogenous YFP-tagged *Rab10* (A-D) or *tj> Rab10-RFP* (E-H). Schemes represent the back half of a follicle cell with the localization of Rab10 (magenta) at the basal (right), sup-basal (center), and middle cell levels (left). Black arrow indicates the direction of follicle rotation. (I) Basal view of stage 8 follicles expressing endogenous Dys-sfGFP (green). F-actin is visualized in magenta. (J, K) Basal (J-J’’’) or sup-basal (K-K’’’) of stage 8 follicles that express endogenous *Dys-sfGFP* (green) and *tj> Rab10-RFP* (magenta). Schemes represent the back half of a follicle cell with the localization of actin or Rab10 (magenta) and Dys (green) at the basal (top and middle) or sup-basal plan (bottom). Scale bars, 5 µm.

Figure 5: DAPC is sufficient to recruit the Rab10-dependent route

A-D) Basal view of the BM in stage 8 *Col IV-GFP* -expressing follicles of the following genotypes (A) *tj> Rab10-RFP (Rab10* OE*)* (B) *tj >Rab10-RFP ; Dys* (C) *tj,>Rab8 RNAi (Rab8 KD)*, (D) *tj, >Rab8 RNAi; Dys*. Scale bars, 10 µm. (E) Quantifications of BM fibril fraction (%) in stage 8 follicles of the indicated genotypes (n = 12, 11, 15, 11, 10 follicles). (F-I) Cross-sections of stage 8 *Col IV-GFP*-expressing follicles of the following genotypes: (F) *tj>Rab10 RNAi (Rab10 KD)*, G) *tj>Rab10 RNAi; Dys*, (H) *tj>Rab8* RNAi, (I), *tj>Rab8 RNAi; Dys.* Images show Col IV-GFP (green, bottom; white, top) and F-actin (magenta). Scale bar, 10 µm. (J) Apical fraction quantification (%) of Col IV-GFP fluorescence intensity in stage 8 follicles of the indicated genotypes (n = 7, 8, 7, 6, 7 follicles). (K-N) Basal and (K’-N’) sup-basal views of stage 8 follicles of the following genotypes: (K) *tj> Dg-GFP* (DG-GFP overexpression (OE), (L) *tj> Dg; Dys-sfGFP*, (M) *tj> Dg-GFP > Rab10-RFP*, (N) *tj> Dg-GFP> Rab10-RFP*; *Dys*. Dg is labelled in white, Dys in green, and Rab10 in magenta. Scale bars, 5 µm. (O-Q) Quantification of (O) Dg-GFP, (P) Dys-sfGFP and (Q) Rab10-RFP mean signal intensity at the trailing edge vs adjacent lateral sides of follicle cells of the indicated genotypes, on 0.45 µm projections starting 0.15 µm below the basal surface; n =68, 59, 50 follicle cells (O), n=72, 83, follicle cells (P), n=60, 62, 55 follicle cells (Q). (R-S)

Representative images of F-actin and Col IV-GFP in (R) control and (S) Dg-overexpressing follicle cells in a plan in the middle of the cells. Note the presence of large BM fibrils between cells (white arrows) and the aberrant shape of cells in S. Scale bars, 10 µm. ****p <0.0001, ns: not significant (one-way ANOVA with Kruskal-Wallis comparisons test for E,J,O,Q, and Mann-Whitney test for P). In all graphs, data are the mean ± SD.

Figure 6: Exo70 interacts with and limits the planar polarization of dystrophin

(A) Representative scheme of Dys domains and the fragments identified in a yeast two-hybrid screen with Exo70 as prey. These fragments encompass a minimal region that includes some spectrin repeats (SR 22 and 23). (B) GST pull-down experiments between GST (left) or GST-SR22-23 (right) and S^{35}-labeled Exo70. (C-E, G-I). Sup-basal view of stage 8 follicles that express (C-E) endogenous *Dys-sfGFP* (green) or (G-I) *tj>Rab10-YFP* (green), in (C, G) control, (D, D', H, H') *tj> Scarlet-Exo70* (Exo OE; magenta) or (E, I) *Exo70* null mutant. Scale bars, 5 µm. Note that Scarlet-Exo70 is expressed in a mosaic manner and that Dys lateral delocalization fits with this expression pattern. (F, J) Quantification of Dys-GFP (F) and Rab10-YFP (J) mean signal intensity at the trailing edge vs adjacent lateral sides of follicle cells of the indicated genotypes, on 0.45 µm projections starting 0.15 µm below the basal surface; n = 112, 45, 89 follicle cells (F), n=108, 28, 124 follicle cells (J). (K) Schemes represent the back half of follicle cells with the localization of Dys (green) and Rab10 (magenta) at the sup-basal surface in control (left), *Exo70* OE (middle) and *Exo70* null mutant. (L-O) Basal view of the BM at stage 8 in (L) control, (M) *Dys* null mutant, (N) *Exo70* null mutant, (O) double *tj>Exo70* RNAi (Exo KD)-*Dys* null mutant follicles visualized with Col IV-GFP. Scale bars, 10 µm. (P) Quantification of BM fibril fraction (%) in stage 8 follicles of the indicated genotypes. In order on the graph, n = 10, 12, 12, 12, 8 follicles. Data are the mean ± SD; *p <0.05, **p <0.01****, p <0.0001 (one-way ANOVA with the Kruskal-Wallis comparisons test for F and J and with Dunnett's multiple comparisons test for P).

Figure 7: Exocyst is required for the Rab8 dependent route

(A) Projection of lateral (A-A') and basal (A'') focal planes or color-coded z projections in function of the z axis of the lateral and basal focal planes used for BM secretion quantification (A''') in *Exo70* null mutant individual single-cell clones that express Col IV-GFP (green, top) and stained for F-actin (magenta) and GFP (white). Scale bars, 5 µm. (B) Quantification of the planar orientation of the lateral BM protein secretion in *Exo70* null mutant single cells. (C) Quantification of the lateral fraction of BM secretion (%) in control and *Exo70* null mutant single-cell clones. In order on the graph, n= 28 and 13 cells. Unpaired t test. (D) Quantification of the BM fibril fraction (%) in stage 8 follicles of the indicated genotypes. In order on the graph, n = 10, 10, 13, 16, 14 follicles. (E-G) Cross-sections of stage 8 follicles of the indicated genotypes: (E) *tj> Exo70 RNAi,* (F) *tj> Rab10 RNAi*, (G) *tj > Exo70 RNAi > Rab10 RNAi.* Images

show Col IV-GFP (white, left; green, right) and F-actin (magenta) localization. Scale bar, 10 µm. (H) Quantification of the ratio between apical and basal Col IV-GFP fluorescence intensity (%) in stage 8 follicles of the indicated genotypes. In order on the graph, n =6, 7, 3, 7 follicles. (I) Quantification of Dys-GFP mean signal intensity at the trailing edge vs adjacent lateral sides in control and *Rab8* KD follicle cells. In order on the graph, n = 85 and 96 follicle cells. For all graphs, data are the mean ± SD. *p <0.05, ****p <0.0001 (one-way ANOVA with Dunnett's multiple comparisons test for D, and with Tukey's multiple comparisons test for H; Mann-Whitney test for I).

SUPPLEMENTAL INFORMATION

Figure S1

(A) Projections of the apical region of stage 8 follicles that capture some of the apical surface due to the tissue curvature showing the ectopic Col IV-GFP (white, top; green, bottom) and F-actin (white, middle; magenta, bottom) in follicular epithelia of the indicated genotypes: *Rab8* KD (left), *Rab10* KD (middle), *Rab8-Rab10* double KD (right). (B) Cross-sections of stage 8 follicles of the indicated genotypes (control, *Rab8-Rab10* double KD, *Rab11* KD, *Rab8-Rab10-Rab11* triple KD, showing aPKC (magenta, top; white, bottom) and Col IV-GFP (green).

Figure S3

Basal view of the BM at stage 8 in *Col IV-GFP* and *tj> Cg25c-GFP* follicle cells.
Quantifications of BM fibril fraction (%) in stage 8 follicles of the indicated genotypes. Data are the mean ± SD; ns, not significant (unpaired t test). In order on the graph, n = 10, 9 follicles.

Figure S4

(A-C') Basal (C, C'), sup-basal (i.e. 0.4 µm above the basal surface) (B, B') and middle (i.e. 0.8 µm below basal surface) (A, A') views of stage 8 follicles that overexpress RFP-tagged *Rab10* (magenta) and endogenous Col IV-GFP (green). (D-D'') Basal view of stage 8 follicles treated with collagenase before fixation to visualize intracellular endogenous basal Col IV-GFP (green) and Rab10-RFP (magenta). (E-E'') Basal view of a photobleached window at the surface of stage 8 living follicles taken 20 minutes after photobleaching to visualize intracellular basal Rab10-RFP (magenta) and endogenous Col IV-GFP (green) expression in non-bleached cells that have migrated in the bleached BM area. Scale bars, 5 µm.

Figure S5

(A-A') Basal and (A'',A''') sup-basal view of stage 8 follicles expressing *Rab10*-RFP (magenta) in WT cells (GFP cells, green) or in *Dys* null mutant cell clones (no GFP). (B) Rab10-RFP mean signal intensity at the trailing edge vs adjacent lateral sides of follicle cells of the indicated genotypes, on 0.45 µm projections starting 0.15 µm below the basal surface. Data are the mean ± SD. (C) Quantification of the lateral fraction of BM secretion (%) in single-cell clones overexpressing Col IV-GFP in control and *Dys* null mutant follicle. Data are the mean ± SD; **p <0.01 (one-way ANOVA). (H-J) Quantification of the planar orientation of lateral BM protein secretion from individual single-cell clones in control (red) and *Dys* null mutant (blue).
(E-G) Sagittal view of follicles (E) overexpressing *Dg*-GFP (white) or expressing endogenous *Dys*-sfGFP (green) in (F) WT context or in (G) *Dg* overexpression (E'-G') F-actin in magenta (H-I) Basal or sup-basal view of Dg-GFP in stage 8 follicles of indicated genotypes : *tj> Dg-GFP > Rab10-RFP* (F) and *tj> Dg-GFP > Rab10-RFP* ; *Dys* mutant (H). Scale bars, 5 µm in (A, C-E), 10µm

in (F-G). (H,I) basal and (H',I') sup-basal images of tj>Dg-GFP in (H) WT or (I) *Dys* mutant conditions. J) Quantifications of BM fibril fraction (%) of stage 8 WT or *tj> Dg* follicles. Data represent mean ± SD. Unpaired t test, *p < 0.05. In order on graph, n = 14 and 11 follicles. (K-L) Basal and (K', L') sup-basal views of the BM on stage 8 control (K) and *tj> Dg* (L)) follicles visualized with Col IV-GFP (green). (H, I) Mann-Whitney test, ****p < 0.0001

Figure S6

(A) Quantifications of BM fibril fraction (%) in stage 8 follicles of the indicated genotypes. In order on the graph, n = 12, 9, 8, 9, 12, 9, 9, 12 and 10 follicles. (B-D) Basal view of the BM visualized with Col IV-GFP at stage 8 in (B) control, (C) *Exo70* null mutant, (D) *Exo70* null mutant with *Exo70 OE* follicles. Scale bars, 10 µm. (E) Quantification of BM fibril fraction (%) in stage 8 follicles of the indicated genotypes. In order on the graph, n = 13, 11, 11 follicles. For all graphs, data are the mean ± SD; ***p <0.01, ****p <0.0001 (one-way ANOVA in A, and one-way ANOVA with Kruskal-Wallis comparisons test in E).

Table S1: Resources and reagents

RESOURCE OR REAGENT	SOURCE	IDENTIFIER
Experimental models: Organisms/Strains		
tj:Gal4 : P{w+mW.hs=GawB}NP1624	Kyoto Stock Center (DGRC)	FlyBase ID: FBti0034540; DGRC: 104055
collV-GFP : P{PTT-un1} vkg G205	Kyoto Stock Center (DGRC)	FlyBase ID: FBti0074199; DGRC: 110626
tub:Gal80ts : P{w[+mC]=tubP-GAL80[ts]}20	Bloomington Drosophila Stock Center	FlyBase ID: FBti0027796; BDSC: 67059
Rab10 RNAi : UAS:Rab10(JF02058)	Bloomington Drosophila Stock Center	FlyBase ID: FBal0220549; BDSC: 26289
Rab8 RNAi : UAS:Rab8(GD12520)	Vienna Drosophila Resource Center	FlyBase ID: FBal0208212; VDRC: 28092
Rab11 RNAi : UAS:Rab11(KK108297)	Vienna Drosophila Resource Center	FlyBase ID: FBal0235482; VDRC: 108382
UAS:Rab10-RFP (chr2)	Isabella and Horne-Badovinac, 2016	

UAS:Rab10-RFP (chr3)	Isabella and Horne-Badovinac, 2016	
UAS:Rab8-YFP : UASp-YFP.Rab8}45	Bloomington Drosophila Stock Center	FlyBase ID: FBti0100806; BDSC: 9782
UAS:LacZ : P{UAS-lacZ.NZ}J312	Bloomington Drosophila Stock Center	FlyBase ID: FBti0012289 BDSC: 3956
UAS:Cg25c-GFP	V. Van De Bor gift	FlyBase ID: FBal0336357
Rab10-eYFP ki : TI (Tiainen et al, 1999)Rab10[EYFP]	Bloomington Drosophila Stock Center	FlyBase ID: FBti0178272; BDSC: 62548
Dys::sfGFP::LoxP	this study	
UAS:Dg-GFP	Marie Laure Parmentier gift	FlyBase ID: FBal0244402
UAS:Dg	(Deng et al, 2003) (Ruhola-Baker lab)	FlyBase ID: FBal0145088
Dys^{E17}	Christoforou 2008} (Rob Ray)	FlyBase ID: FBal0241311
$Dys_{Exel6184}$: FRT 82B, Df(3R)Exel6184	Bloomington Drosophila Stock Center	FlyBase ID: FBab0038239; BDSC: 7663
y,w, hs:FLP : P{ry[+t7.2]=hsFLP}22, w[*]	Bloomington Drosophila Stock Center	FlyBase ID: FBst0008862; BDSC: 8862
y,w, hs:FLP : P{ry[+t7.2]=hsFLP}1, w[1118]	Bloomington Drosophila Stock Center	FlyBase ID: FBti0002044 or BDSC: 6
FRT82B	Bloomington Drosophila Stock Center	FlyBase ID: FBti0002074; BDSC: 2035
P{y[+t7.7] w[+mC]=CoinFLP-GAL4}attP	Bloomington Drosophila Stock Center	FlyBase ID: FBtp0096005; BDSC: 58750
$Exo70^{MB04553}$	Bloomington Drosophila Stock Center	FlyBase ID: FBti0078291; BDSC: 24721

Df(3L)BSC815	Bloomington Drosophila Stock Center	FlyBase ID: FBab0045927; BDSC: 27576
Exo70 RNAi : Exo70(KK101154)	Vienna Drosophila Resource Center	FlyBase ID: FBal0231092; VDRC: 103717
Exo70 RNAi : Exo70(GD12140)	Vienna Drosophila Resource Center	FlyBase ID: FBal0209535; VDRC: 27867
Sec3 RNAi : Sec3(GD10687)	Vienna Drosophila Resource Center	FlyBase ID: FBal0210549; VDRC: 35806
Sec5 RNAi : Sec5(GLC01676)	Bloomington Drosophila Stock Center	FlyBase ID: FBal0291964; BDSC: 50556
Sec6 RNAi : Sec6(KK102544)	Vienna Drosophila Resource Center	FlyBase ID: FBal0231852; VDRC: 105836
Sec8 RNAi : Sec8 (GD8828)	Vienna Drosophila Resource Center	FlyBase ID: FBal0210555; VDRC: 45032
Sec10 RNAi : Sec10(JF02633)	Bloomington Drosophila Stock Center	FlyBase ID: FBal0242222; BDSC: 27483
Sec15 RNAi : Sec15(GD12109)	Vienna Drosophila Resource Center	FlyBase ID: FBal0210546; VDRC: 35161
Exo84 RNAi : Exo84(KK100045)	Vienna Drosophila Resource Center	FlyBase ID: FBal0230555; VDRC: 108650
UAS: YFP Rab8 (chr 3)	Bloomington	Bl#23272
UAS: Scarlet-Exo70	this study	
Antibodies		
anti-GFP, goat	Abcam	5450; dilution 1/1000
anti-aPKc, goat	Santa Cruz Biotechnology	Sc-216-g dilution 1/500
anti-goat-Cy5, Donkey	Jackson Immunoresearch	705-175-147; dilution 1/1000

Anti-goat-Cy3, Donkey	Jackson Immunoresearch	705-165-147; dilution 1/1000
Chemicals, Peptides, and Recombinant Proteins		
Phalloidin Atto-488, -550, -633	Sigma	#49409, #19083, #68825
Collagenase	Worthington Biochemical Corporation	# LS005273
Software and Algorithms		
Fiji	(Schindelin et al, 2012)	
R		
Prism		

Table S2: Genotypes and specific conditions

(h: hours; HS: heat-shock)

Figure	Genotype	Condition
Figure 1 B-H	*tj:Gal4, colIV-GFP, tub:Gal80^{ts} / CyO* *tj:Gal4, colIV-GFP, tub:Gal80^{ts} / UAS:Rab8 RNAi* *tj:Gal4, colIV-GFP, tub:Gal80^{ts} /+; UAS:Rab10 RNAi /+* *tj:Gal4, colIV-GFP, tub:Gal80^{ts} / UAS:Rab8 RNAi; UAS:Rab10 RNAi /+* *tj:Gal4, colIV-GFP, tub:Gal80^{ts} / UAS:Rab11 RNAi* *tj:Gal4, colIV-GFP, tub:Gal80^{ts} / UAS:Rab8 RNAi, UAS:Rab11 RNAi; UAS:Rab10 RNAi /+*	18°C, 48h 30°C
Figure S1 A	*tj:Gal4, colIV-GFP, tub:Gal80^{ts} / UAS:Rab8 RNAi* *tj:Gal4, colIV-GFP, tub:Gal80^{ts} /+; UAS:Rab10 RNAi /+* *tj:Gal4, colIV-GFP, tub:Gal80^{ts} / UAS:Rab8 RNAi; UAS:Rab10 RNAi /+*	18°C, 48h 30°C
B	*tj:Gal4, colIV-GFP, tub:Gal80^{ts} / CyO* *tj:Gal4, colIV-GFP, tub:Gal80^{ts} / UAS:Rab8 RNAi; UAS:Rab10 RNAi /+* *tj:Gal4, colIV-GFP, tub:Gal80^{ts} / UAS:Rab11 RNAi* *tj:Gal4, colIV-GFP, tub:Gal80^{ts} / UAS:Rab8 RNAi, UAS:Rab11 RNAi; UAS:Rab10 RNAi /+*	18°C, 48h 30°C
Figure 2 B-H	*tj:Gal4, colIV-GFP / CyO* *tj:Gal4, colIV-GFP /+; UAS:Rab10-RFP /+* *tj:Gal4, colIV-GFP /+; UAS:Rab10 RNAi /+*	30°C

	tj:Gal4, colIV-GFP / UAS:Rab8-YFP *tj:Gal4, colIV-GFP / UAS:Rab8 RNAi* *tj:Gal4, colIV-GFP / UAS: Rab8-YFP; UAS:Rab10-RFP /+*	
I	*tj:Gal4, colIV-GFP / +; UAS:LacZ /+* *tj:Gal4, colIV-GFP/ UAS:Rab8-YFP; UAS:LacZ /+* *tj:Gal4, colIV-GFP /+; UAS:LacZ / UAS:Rab10-RFP* *tj:Gal4, colIV-GFP / UAS:Rab8-YFP; UAS:Rab10-RFP /+*	30°C
Figure 3 B-J	*hs:flp1; Act5c CoinFLP-Gal4/UAS:colIV-GFP* *hs:flp1; Act5c CoinFLP-Gal4/UAS:colIV-GFP UAS:Rab10-RFP /+* *hs:flp1; Act5c CoinFLP-Gal4/UAS:colIV-GFP UAS:Rab8-YFP /+*	25°C, HS 15 min 37°C, 30°C 9h
Figure S3	*tj:Gal4, colIV-GFP / CyO* *tj:Gal4 / UAS:Cg25c-GFP*	25°C
Figure 4 A-D	*Rab10-eYFP ki*	25°C
E-H	*tj:Gal4, colIV-GFP /+; UAS:Rab10-RFP /+*	25°C
I	*Dys-sfGFP*	25°C
J-K	*tj:Gal4 /+; UAS:Rab10-RFP / Dys-sfGFP*	25°C
Figure S4	*tj:Gal4, colIV-GFP /+; UAS:Rab10-RFP /+*	25°C
Figure 5 A-J	*tj:Gal4, colIV-GFP /+; Dys^{E17} / $Dys^{Exel6184}$* *tj:Gal4, colIV-GFP / UAS:Rab10-RFP* *tj:Gal4, colIV-GFP / UAS:Rab10-RFP; Dys^{E17} / $Dys^{Exel6184}$* *tj:Gal4, colIV-GFP / UAS:Rab8 RNAi* *tj:Gal4, colIV-GFP / UAS:Rab8 RNAi; Dys^{E17} / $Dys^{Exel6184}$* *tj:Gal4, colIV-GFP / UAS:Rab10-RNAi* *tj:Gal4, colIV-GFP / UAS:Rab10 RNAi; Dys^{E17} / $Dys^{Exel6184}$*	25°C, 30°C 72h
K	*tj:Gal4 / UAS: Dg-GFP*	25°C, 30°C 48h
L	*tj:Gal4 / UAS:Dg; Dys-sfGFP /+*	25°C, 30°C 72h
M	*tj:Gal4 / UAS:Dg-GFP; UAS:Rab10-RFP /+*	25°C, 30°C 72h
N	*tj:Gal4 /UAS:Dg-GFP; UAS:Rab10-RFP, Dys^{E17}/$Dys^{Exel6184}$*	25°C, 30°C 72h
O	*tj:Gal4 / UAS: Dg-GFP* *tj:Gal4 / UAS:Dg-GFP; UAS:Rab10-RFP /+* *tj:Gal4 /UAS:Dg-GFP; UAS:Rab10-RFP, Dys^{E17}/$Dys^{Exel6184}$*	25°C, 30°C 72h

P	*Dys-sfGFP* *tj:Gal4 / UAS:Dg; Dys-sfGFP /+*	25°C, 30°C 72h
Q	*tj:Gal4 /+; UAS:Rab10-RFP /+* *tj:Gal4 / UAS:Dg-GFP; UAS:Rab10-RFP /+* *tj:Gal4 /UAS:Dg-GFP; UAS:Rab10-RFP, Dys^{E17}/$Dys^{Exel6184}$*	25°C, 30°C 72h
R-S	*tj:Gal4, colIV-GFP /+* *tj:Gal4, colIV-GFP / UAS:Dg*	25°C, 30°C 72h
Figure S5 A-B	*y,w,hs:flp122; tjGal4 / UAS:Rab10-RFP; FRT82B-GFP / FRT82B, $Dys^{Exel6184}$*	25°C, 2HS 1h, dissection 72h after HS
C-D	*hs:flp1; Act5c CoinFLP-Gal4/UAS:colIV-GFP* *hs:flp1; Act5c CoinFLP-Gal4/UAS:colIV-GFP; Dys^{E17}/$Dys^{Exel6184}$*	25°C, HS 15 min 37°C, 30°C 9h
E-G	*tj:Gal4 / UAS: Dg-GFP* *Dys-sfGFP* *tj:Gal4 / UAS:Dg; Dys-sfGFP /+*	25°C, 30°C 72h 25°C, 30°C 72h
H-I	*tj:Gal4 / UAS:Dg-GFP* *tj:Gal4 /UAS:Dg-GFP; Dys^{E17}/$Dys^{Exel6184}$*	25°C, 30°C 72h 25°C, 30°C 72h
J-L	*tj:Gal4, colIV-GFP /+* *tj:Gal4, colIV-GFP / UAS:Dg*	
Figure 6 C-J	*Dys-sfGFP /+* *tj:Gal4 / UAS: Scarlet-Exo70; Dys-sfGFP /+* *Dys-sfGFP, $Exo70^{MB04553}$ / Df(3L)BSC815* *tj:Gal4, colIV-GFP / UAS:Rab10-RFP* *tj:Gal4 / UAS: Scarlet-Exo70; UAS:Rab10-RFP / +* *tj:Gal4, colIV-GFP / UAS:Rab10-RFP; $Exo70^{MB04553}$ / Df(3L)BSC815*	25°C
L-P	*tj:Gal4, colIV-GFP /+* *tj:Gal4, colIV-GFP /+; Dys^{E17} / $Dys^{Exel6184}$* *tj:Gal4, colIV-GFP /+; $Exo70^{MB04553}$ / Df(3L)BSC815* *tj:Gal4, colIV-GFP / UAS:Exo70 RNAi; Dys^{E17} / $Dys^{Exel6184}$*	25°C, 30°C 72h 25°C, 30°C 72h 25°C 25°C, 30°C 72h
Figure S6 A	*tj:Gal4, colIV-GFP /+*	25°C, 30°C or

			18°C, 30°C 48h
		tj:Gal4, colIV-GFP/ UAS:Sec3 RNAi	30°C
		tj:Gal4, colIV-GFP/+; UAS:Sec5 RNAi	30°C
		tj:Gal4, colIV-GFP/ UAS:Sec6 RNAi	25°C
		tj:Gal4, colIV-GFP/ UAS:Sec8 RNAi	25°C
		tj:Gal4, colIV-GFP/+; UAS:Sec10 RNAi	18°C, 30°C 48h
		tj:Gal4, colIV-GFP/+; UAS:Sec15 RNAi	25°C
		tj:Gal4, colIV-GFP/ UAS:Exo70 RNAi	30°C
		tj:Gal4, colIV-GFP/ UAS:Exo84 RNAi	25°C
	B-E	*tj:Gal4, colIV-GFP /+*	25°C
		tj:Gal4, colIV-GFP /+; Exo70^{MB04553} / Df(3L)BSC815	
		tj:Gal4, colIV-GFP / UAS: Scarlet-Exo70; Exo70^{MB04553} / Df(3L)BSC815	
Figure 7	A-C	*hs:flp1; Act5c CoinFLP-Gal4/UAS:colIV-GFP*	25°C, HS 15 min
		hs:flp1; Act5c CoinFLP-Gal4/UAS:colIV-GFP; Exo70^{MB04553} / Df(3L)BSC815	37°C, 30°C 9h
			25°C
	D	*tj:Gal4, colIV-GFP /+; Exo70^{MB04553} / Df(3L)BSC815*	25°C, 30°C 72h
		tj:Gal4, colIV-GFP / UAS:Rab8 RNAi	25°C, 30°C 72h
		tj:Gal4, colIV-GFP / UAS:Rab8 RNAi; UAS:Exo70 RNAi / +	25°C
		tj:Gal4, colIV-GFP / UAS:Rab10-RFP	25°C
		tj:Gal4, colIV-GFP / UAS:Rab10-RFP; Exo70^{MB04553} / Df(3L)BSC815	
			25°C, 30°C 72h
	E-H	*tj:Gal4, colIV-GFP /+*	
		tj:Gal4, colIV-GFP / UAS:Exo70 RNAi	
		tj:Gal4, colIV-GFP /+; UAS:Rab10 RNAi	
		tj:Gal4, colIV-GFP / UAS:Exo70 RNAi; UAS:Rab10 RNAi	
			25°C, 30°C 72h
	I	*tj:Gal4, colIV-GFP /+*	
		tj:Gal4, colIV-GFP / UAS:Rab8 RNAi	

Figure 1

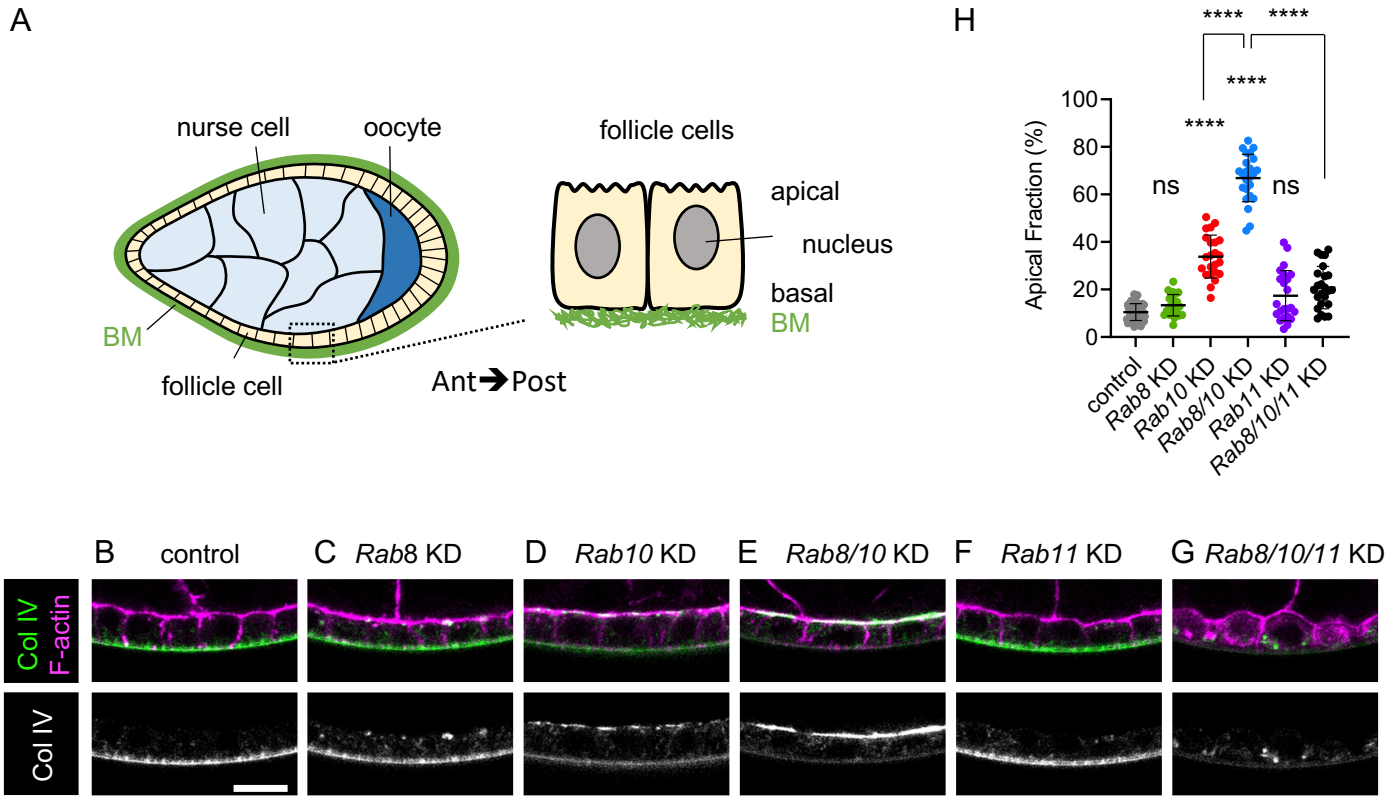
A
nurse cell
oocyte
follicle cells
apical
nucleus
basal
BM
BM
follicle cell
Ant➔Post
H
Apical Fraction (%)
100
80
60
40
20
0
ns
ns
****
****
****
****
control
Rab8 KD
Rab10 KD
Rab8/10 KD
Rab11 KD
Rab8/10/11 KD
B control
C Rab8 KD
D Rab10 KD
E Rab8/10 KD
F Rab11 KD
G Rab8/10/11 KD
Col IV
F-actin
Col IV

Figure S1

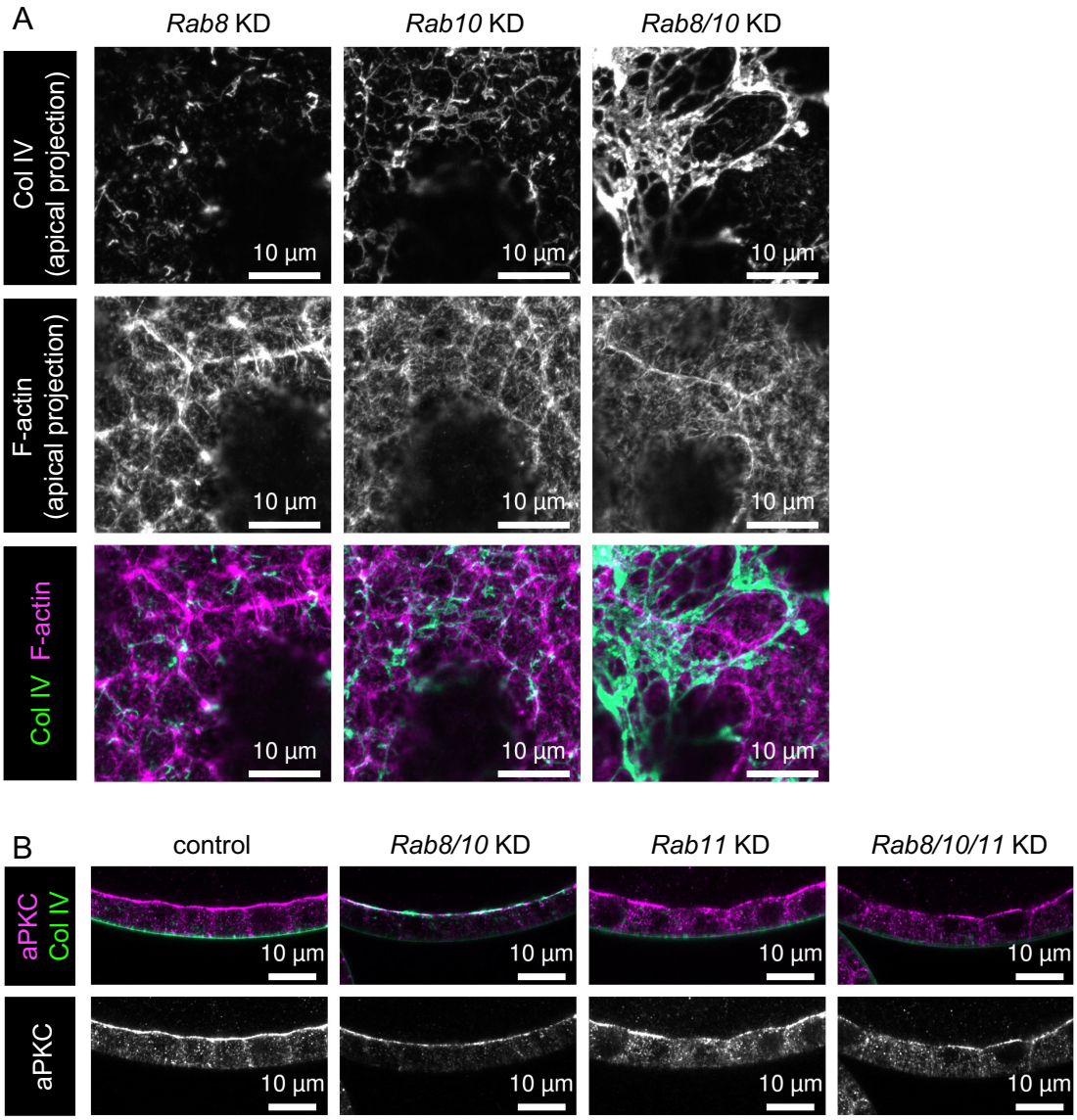
A
Rab8 KD
Rab10 KD
Rab8/10 KD
Col IV (apical projection)
F-actin (apical projection)
Col IV F-actin
10 µm
B
control
Rab8/10 KD
Rab11 KD
Rab8/10/11 KD
aPKC Col IV
aPKC
10 µm

Figure 2

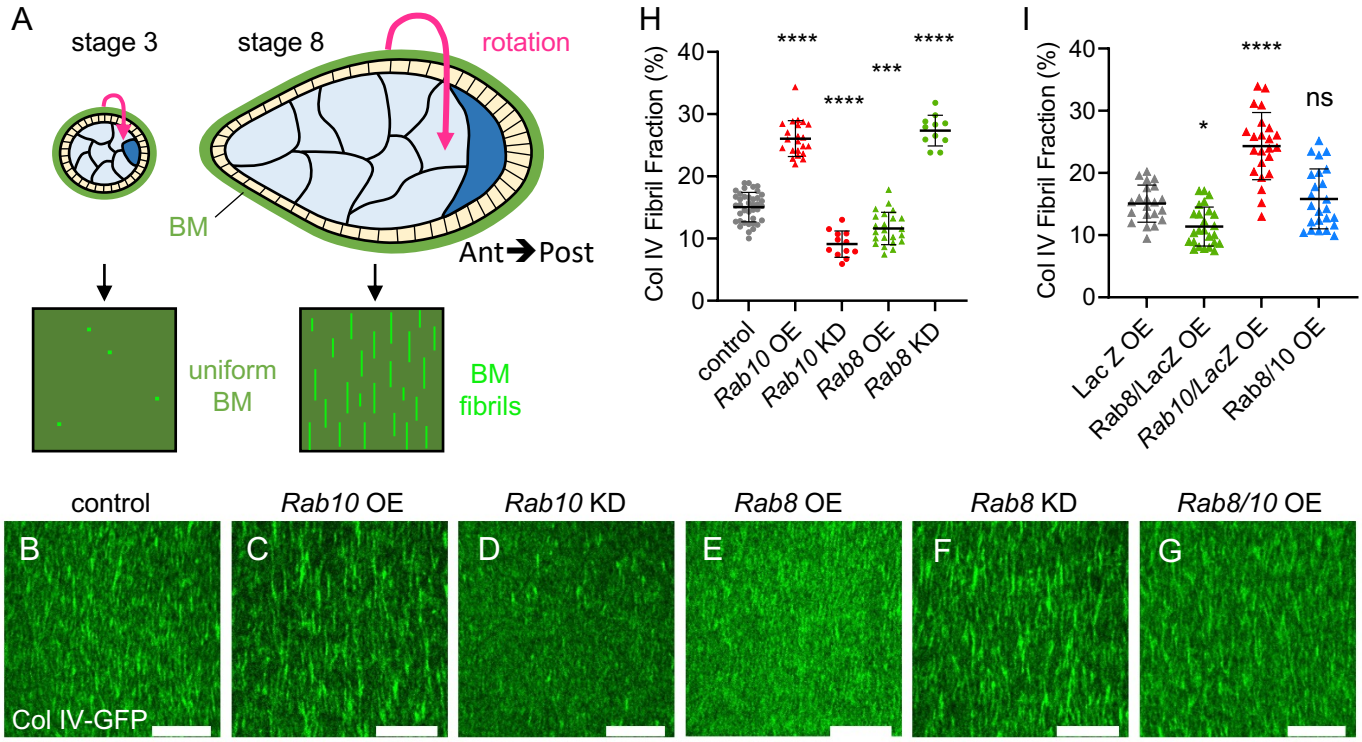
A
stage 3
stage 8
rotation
BM
Ant→Post
uniform BM
BM fibrils
H
Col IV Fibril Fraction (%)
40
30
20
10
0
****
****
***
****
control
Rab10 OE
Rab10 KD
Rab8 OE
Rab8 KD
I
Col IV Fibril Fraction (%)
40
30
20
10
0
*
****
ns
Lac Z OE
Rab8/LacZ OE
Rab10/LacZ OE
Rab8/10 OE
control
Rab10 OE
Rab10 KD
Rab8 OE
Rab8 KD
Rab8/10 OE
B
C
D
E
F
G
Col IV-GFP

Figure 3

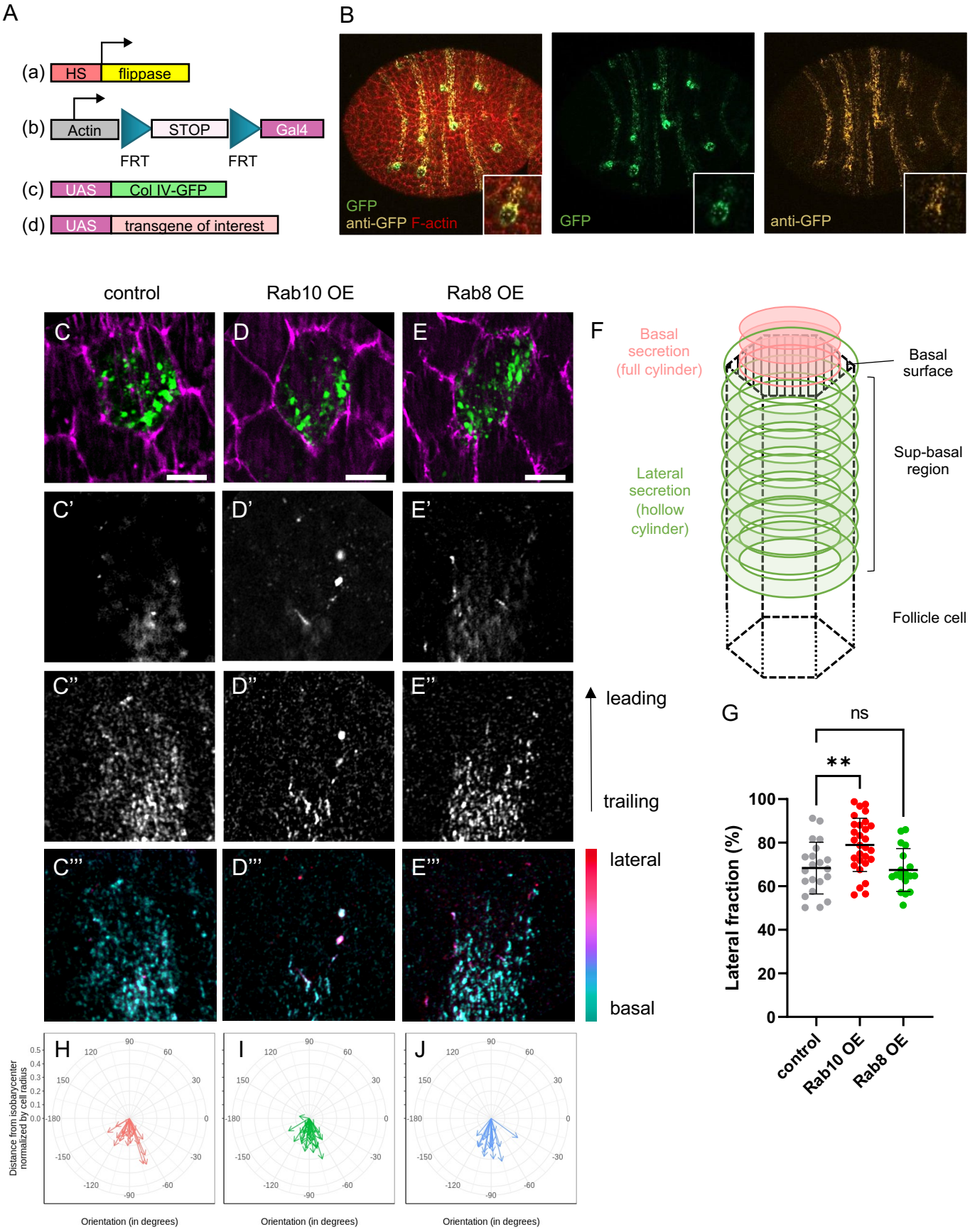
A
(a) HS flippase
(b) Actin STOP Gal4
FRT FRT
(c) UAS Col IV-GFP
(d) UAS transgene of interest
B
GFP
anti-GFP F-actin
GFP
anti-GFP
control
Rab10 OE
Rab8 OE
C
D
E
C'
D'
E'
C''
D''
E''
C'''
D'''
E'''
leading
trailing
lateral
basal
F
Basal secretion (full cylinder)
Lateral secretion (hollow cylinder)
Basal surface
Sup-basal region
Follicle cell
G
ns
**
Lateral fraction (%)
control
Rab10 OE
Rab8 OE
H
I
J
Distance from isobarycenter normalized by cell radius
Orientation (in degrees)
Orientation (in degrees)
Orientation (in degrees)

Figure S3

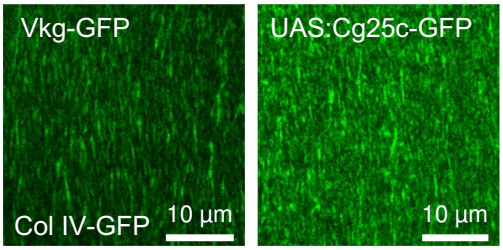
Vkg-GFP
Col IV-GFP
10 µm
UAS:Cg25c-GFP
10 µm

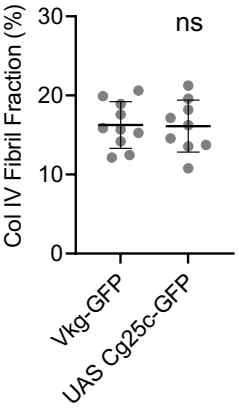
Col IV Fibril Fraction (%)
30
20
10
0
ns
Vkg-GFP
UAS Cg25c-GFP

Figure 4

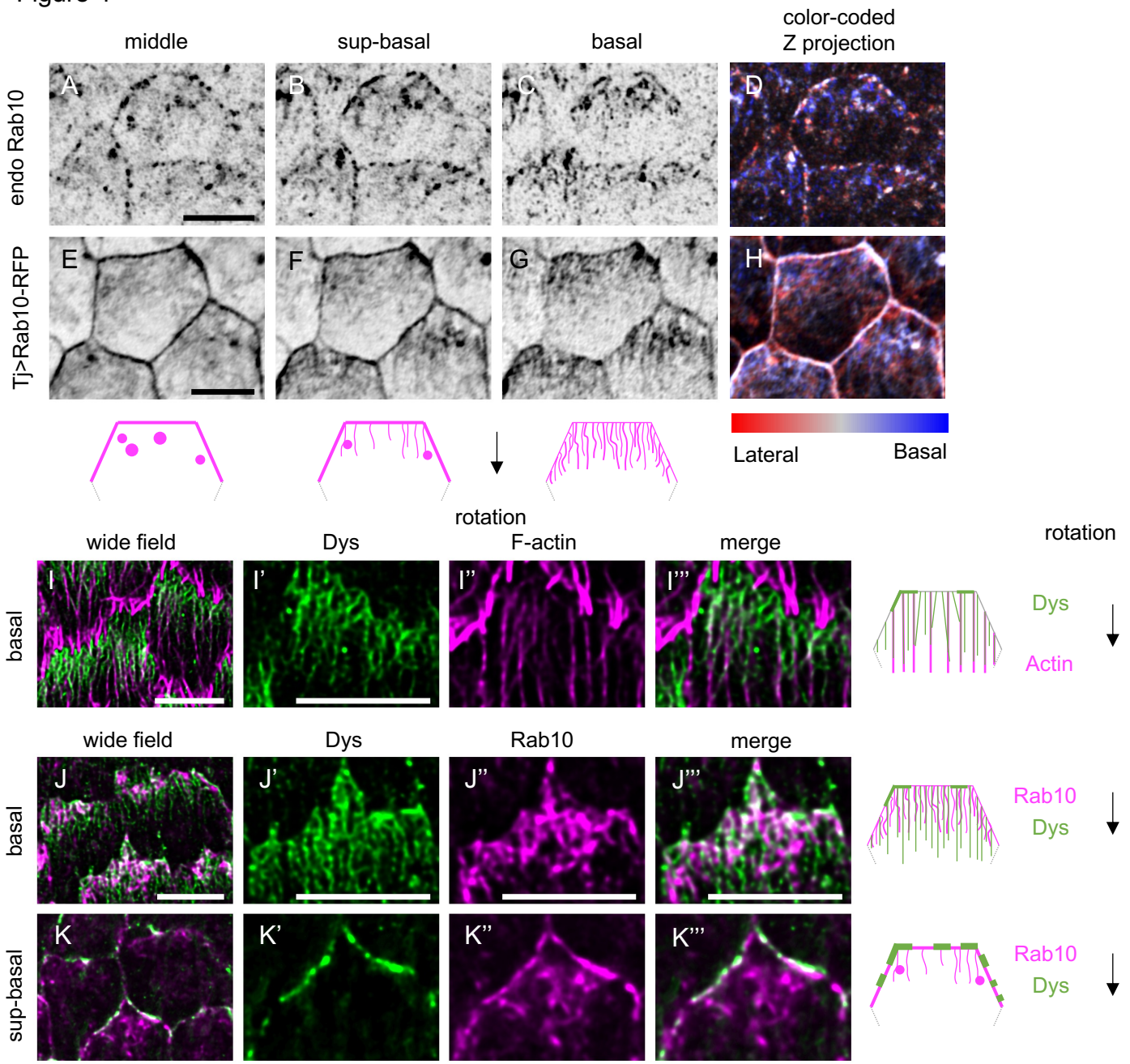
middle
sup-basal
basal
color-coded
Z projection
endo Rab10
Tj>Rab10-RFP
A
B
C
D
E
F
G
H
Lateral
Basal
rotation
wide field
Dys
F-actin
merge
basal
I
I'
I''
I'''
Dys
Actin
rotation
wide field
Dys
Rab10
merge
basal
J
J'
J''
J'''
Rab10
Dys
sup-basal
K
K'
K''
K'''
Rab10
Dys

Figure S4

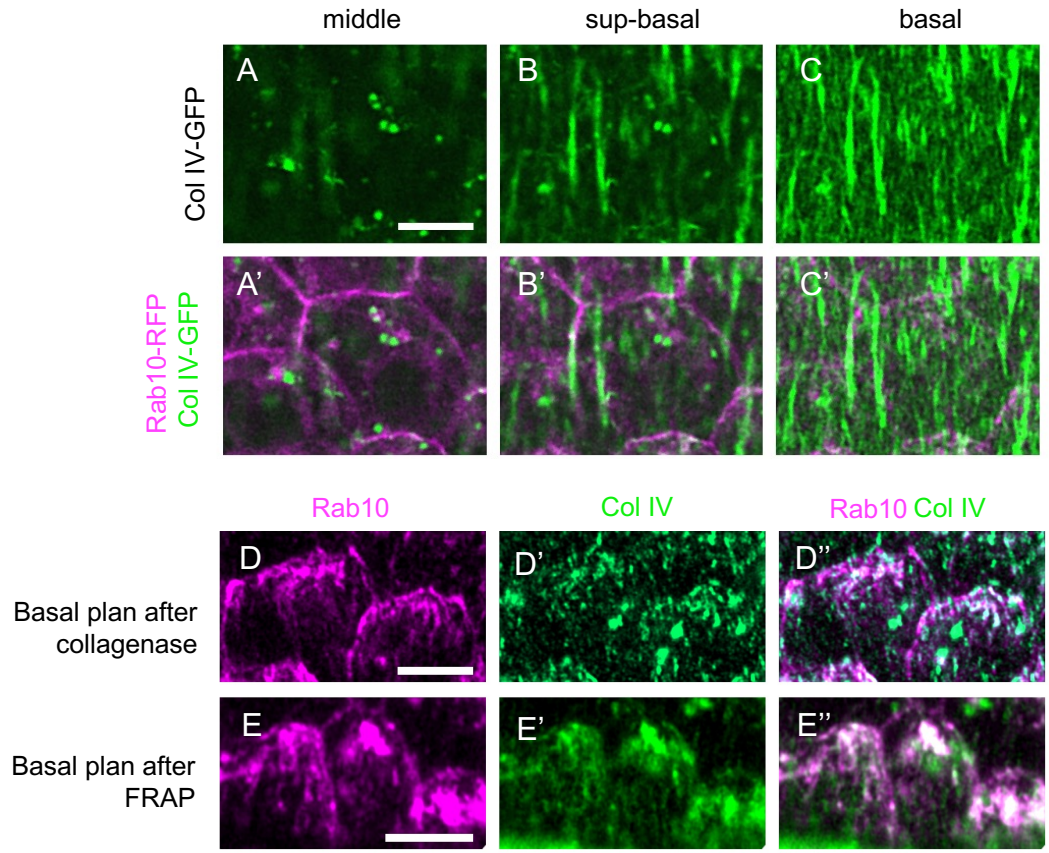
middle
sup-basal
basal
Col IV-GFP
A
B
C
Rab10-RFP
Col IV-GFP
A'
B'
C'
Rab10
Col IV
Rab10 Col IV
Basal plan after collagenase
D
D'
D''
Basal plan after FRAP
E
E'
E''

Figure 5

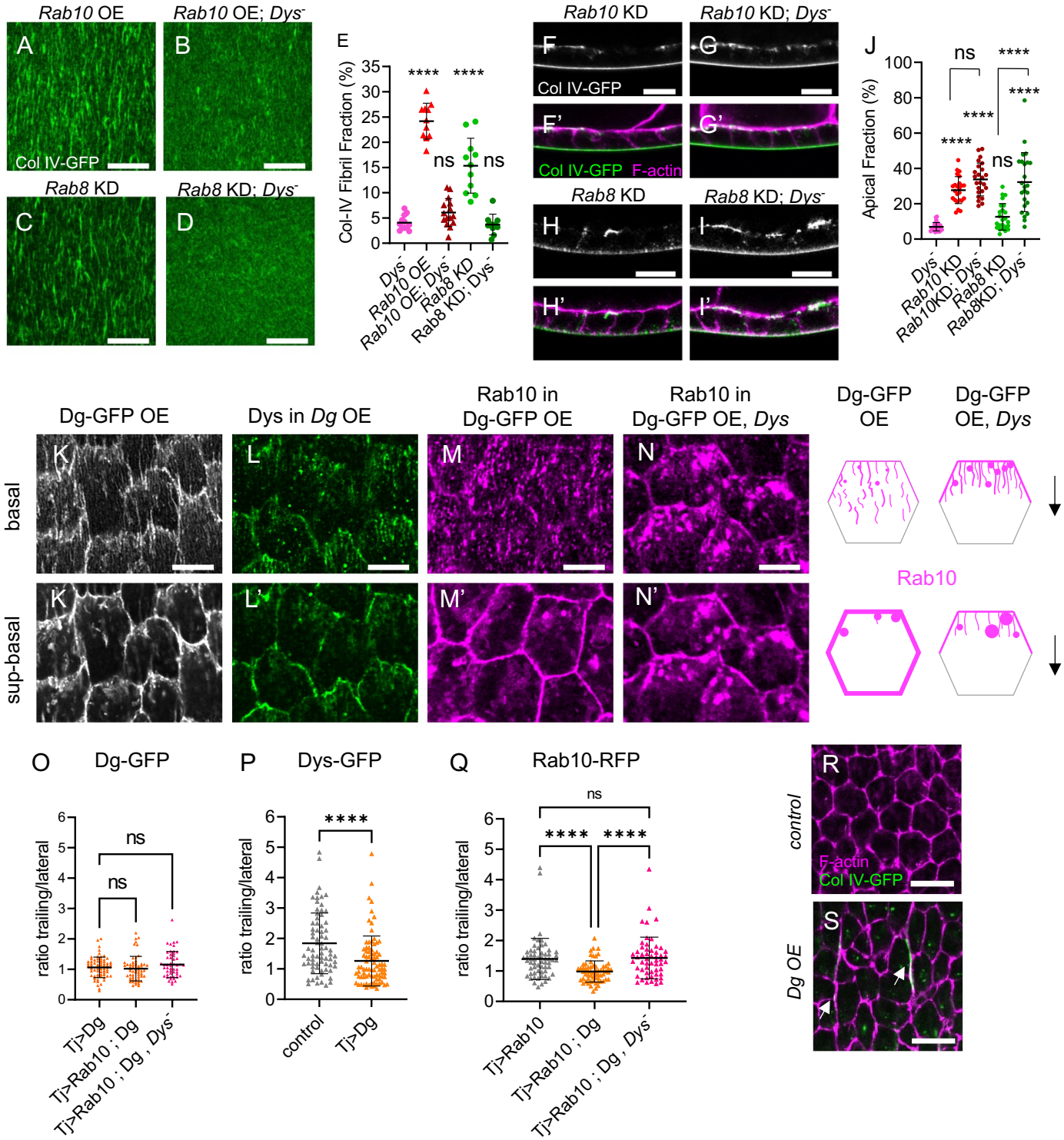
Rab10 OE
Rab10 OE; Dys-
A
B
Col IV-GFP
Rab8 KD
Rab8 KD; Dys-
C
D
E
Col-IV Fibril Fraction (%)
****
****
ns
ns
Dys-
Rab10 OE
Rab10 OE; Dys-
Rab8 KD
Rab8 KD; Dys-
Rab10 KD
Rab10 KD; Dys-
F
G
Col IV-GFP
F'
G'
Col IV-GFP F-actin
Rab8 KD
Rab8 KD; Dys-
H
I
H'
I'
J
Apical Fraction (%)
ns
****
****
****
****
ns
Dys-
Rab10 KD
Rab10KD; Dys-
Rab8 KD
Rab8KD; Dys-
Dg-GFP OE
Dys in Dg OE
Rab10 in Dg-GFP OE
Rab10 in Dg-GFP OE, Dys
Dg-GFP OE
Dg-GFP OE, Dys
basal
sup-basal
K
L
M
N
K
L'
M'
N'
Rab10
O
Dg-GFP
ratio trailing/lateral
ns
ns
Tj>Dg
Tj>Rab10 ; Dg
Tj>Rab10 ; Dg , Dys-
P
Dys-GFP
ratio trailing/lateral
****
control
Tj>Dg
Q
Rab10-RFP
ratio trailing/lateral
ns
****
****
Tj>Rab10
Tj>Rab10 ; Dg
Tj>Rab10 ; Dg , Dys-
control
R
F-actin
Col IV-GFP
Dg OE
S

Figure S5

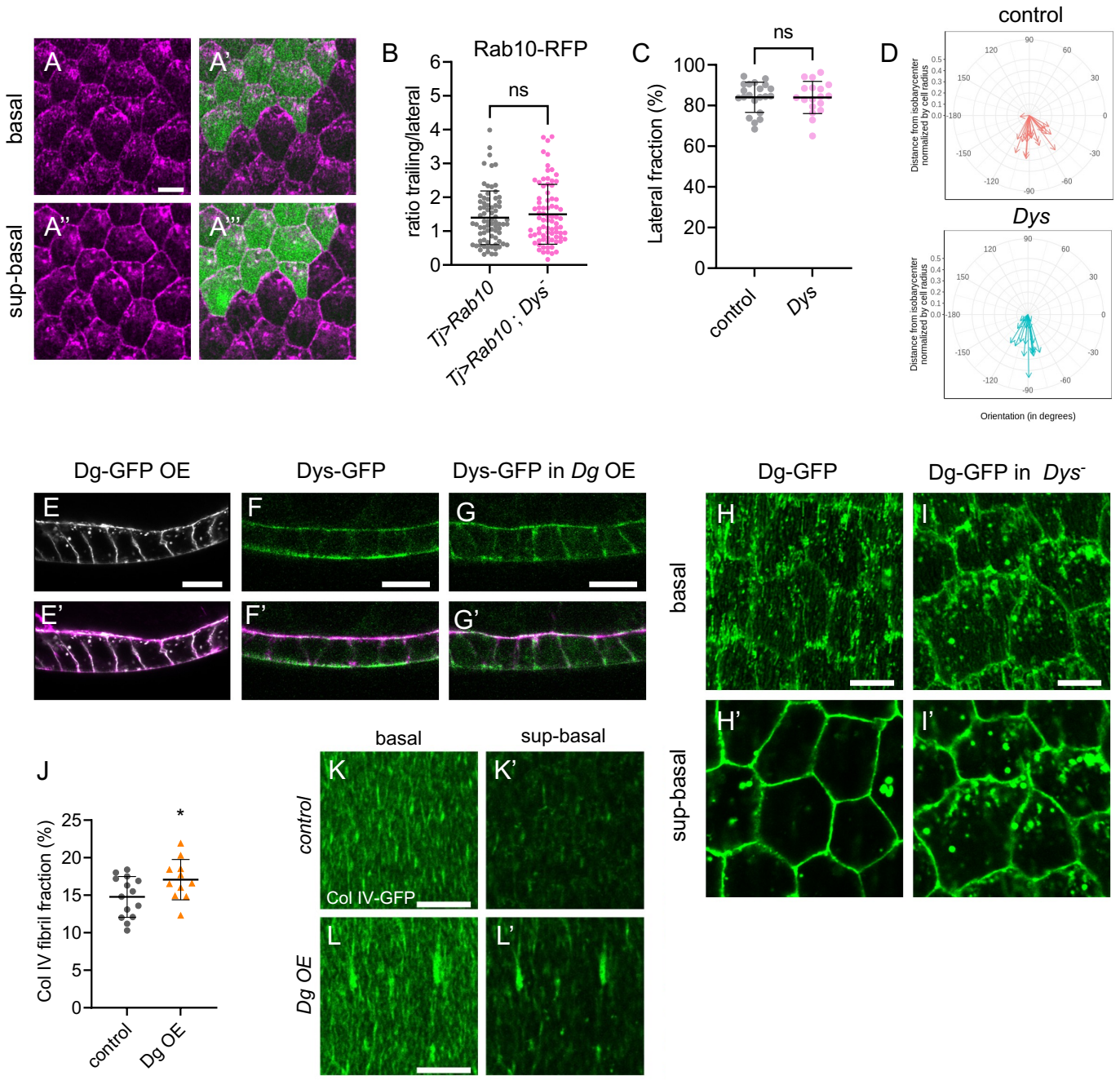
A
A'
A''
A'''
basal
sup-basal
B
Rab10-RFP
ratio trailing/lateral
ns
Tj>Rab10
Tj>Rab10 ; Dys-
C
Lateral fraction (%)
ns
control
Dys
D
control
Dys
Distance from isobarycenter normalized by cell radius
Orientation (in degrees)
Dg-GFP OE
Dys-GFP
Dys-GFP in Dg OE
E
E'
F
F'
G
G'
Dg-GFP
Dg-GFP in Dys-
H
H'
I
I'
basal
sup-basal
J
Col IV fibril fraction (%)
control
Dg OE
basal
sup-basal
K
K'
L
L'
control
Dg OE
Col IV-GFP

Figure 6

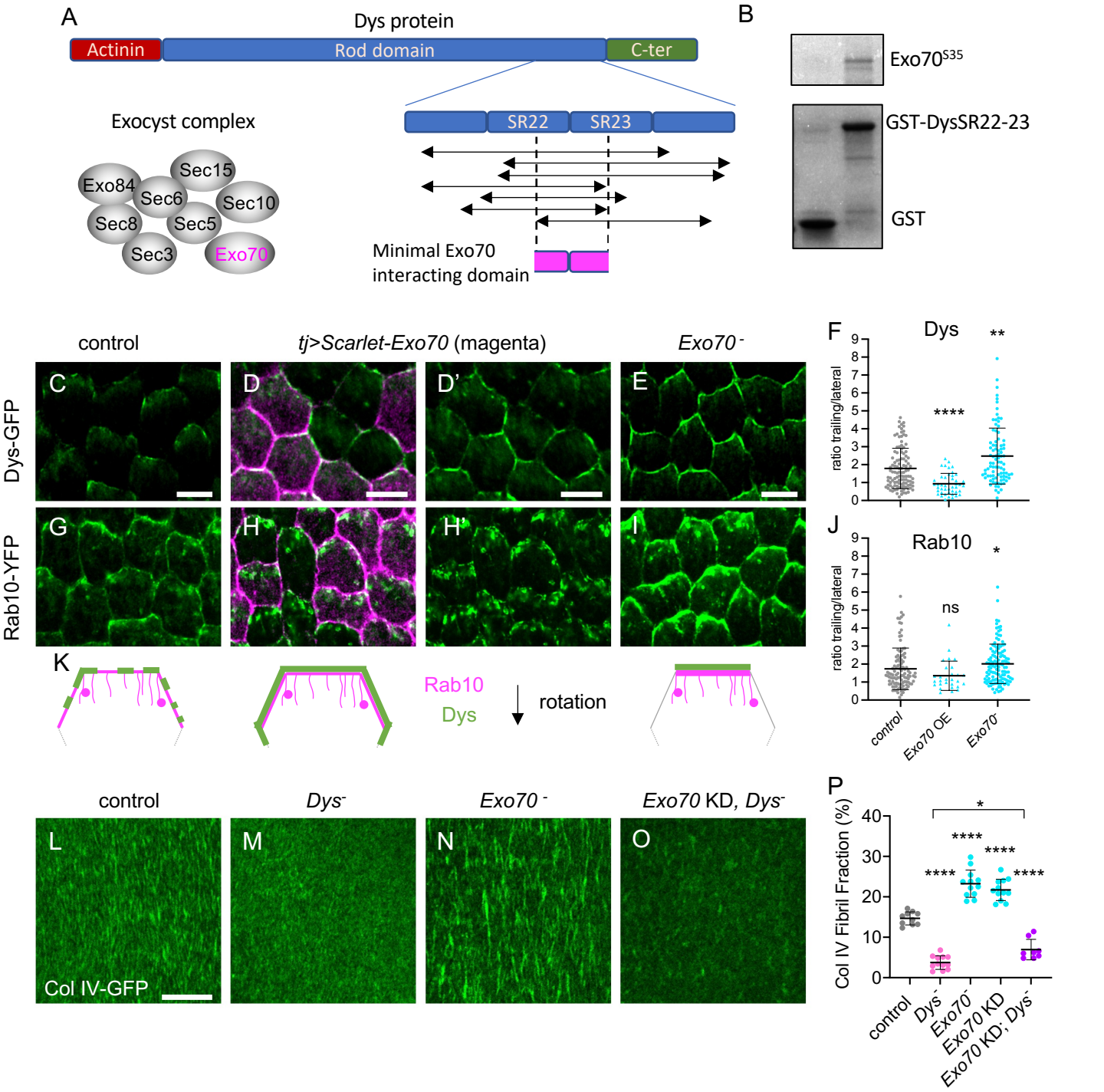
A
Dys protein
Actinin
Rod domain
C-ter
Exocyst complex
Exo84
Sec15
Sec6
Sec10
Sec8
Sec5
Sec3
Exo70
SR22
SR23
Minimal Exo70 interacting domain
B
Exo70S35
GST-DysSR22-23
GST
control
tj>Scarlet-Exo70 (magenta)
Exo70 -
Dys-GFP
Rab10-YFP
C
D
D'
E
G
H
H'
I
K
Rab10
Dys
rotation
F
Dys
ratio trailing/lateral
****
**
J
Rab10
ns
*
control
Exo70 OE
Exo70-
control
Dys-
Exo70 -
Exo70 KD, Dys-
L
M
N
O
Col IV-GFP
P
Col IV Fibril Fraction (%)
*
****
control
Dys-
Exo70-
Exo70 KD
Exo70 KD; Dys-

Figure S6

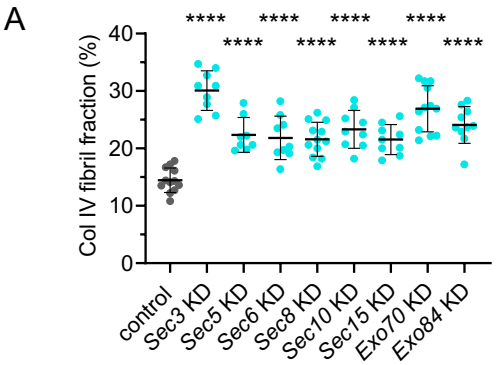
A
Col IV fibril fraction (%)
40
30
20
10
0
****
control
Sec3 KD
Sec5 KD
Sec6 KD
Sec8 KD
Sec10 KD
Sec15 KD
Exo70 KD
Exo84 KD

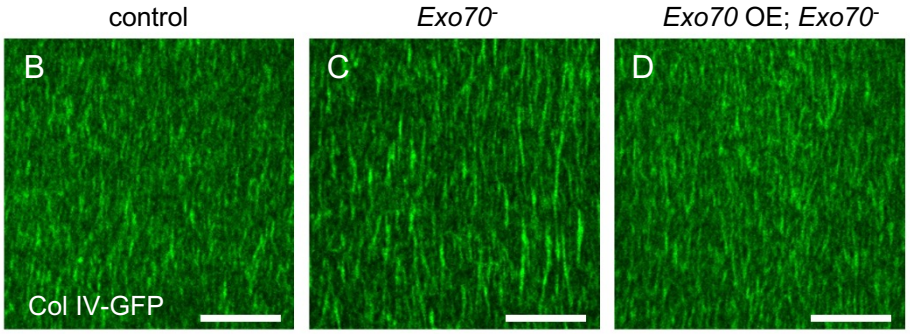
control
Exo70-
Exo70 OE; Exo70-
B
C
D
Col IV-GFP

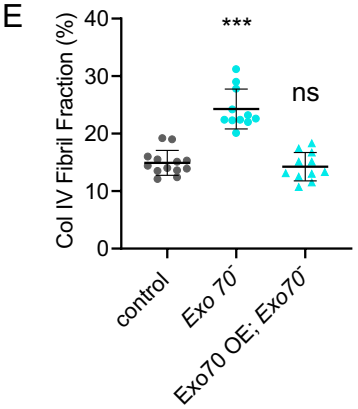
E
Col IV Fibril Fraction (%)
40
30
20
10
0
***
ns
control
Exo 70-
Exo70 OE; Exo70-

Figure 7

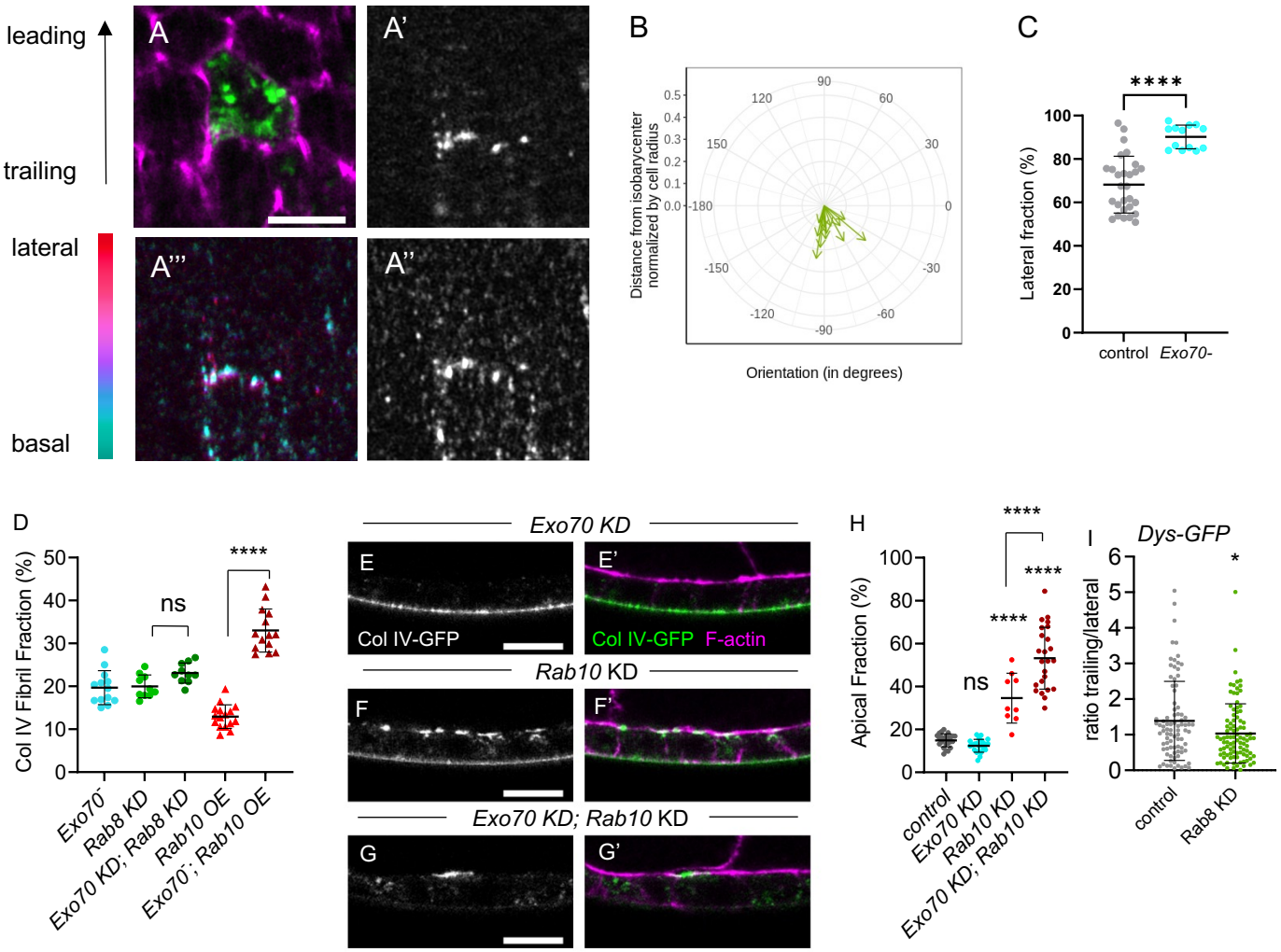
leading
trailing
lateral
basal
A
A'
A'''
A''
B
Distance from isobarycenter normalized by cell radius
Orientation (in degrees)
C
****
Lateral fraction (%)
control
Exo70-
D
Col IV Fibril Fraction (%)
ns
****
Exo70-
Rab8 KD
Exo70 KD; Rab8 KD
Rab10 OE
Exo70-; Rab10 OE
Exo70 KD
E
E'
Col IV-GFP
Col IV-GFP F-actin
Rab10 KD
F
F'
Exo70 KD; Rab10 KD
G
G'
H
Apical Fraction (%)
ns
****
control
Exo70 KD
Rab10 KD
Exo70 KD; Rab10 KD
I
Dys-GFP
ratio trailing/lateral
*
control
Rab8 KD